Escape behaviors in prey might have underlain the evolution of pennaceous plumage in predatory dinosaurs

Piotr Jablonski (piotrjab@behecolpiotrsangim.org)
Seoul National University/Polish Academy of Sciences https://orcid.org/0000-0002-8333-0106
Jinseok Park (winterwren15@gmail.com)
Seoul National University
Minyoung Son (son06229@umn.edu)
Seoul National University/University of Minnesota
Jeongyeol Park (flashpark@g.skku.edu)
Sungkyunkwan University
Sang Yun Bang (babaronka@snu.ac.kr)
Seoul National University
Jungmoon Ha (wjdans1021@gmail.com)
Seoul National University
Hyungpil Moon (hyungpil@g.skku.edu)
Sungkyunkwan University
Yuong-Nam Lee (ynlee@snu.ac.kr)
Seoul National University https://orcid.org/0000-0003-1067-6074
Sang-im Lee (sangim@dgist.ac.kr)
DGIST https://orcid.org/0000-0001-7808-7140

Biological Sciences - Article

Keywords:

DOI: https://doi.org/10.21203/rs.3.rs-2415346/v1

Additional Declarations: There is **NO** Competing Interest.

Escape behaviors in prey might have underlain the evolution of pennaceous plumage in predatory dinosaurs

Authors: Jinseok Park[1], Minyoung Son[2,3], Jeongyeol Park[4], Sang Yun Bang[1], Jungmoon Ha[1], Hyungpil Moon[4*], Yuong-Nam Lee[2*], Sang-im Lee[5*], Piotr, G. Jablonski[1,6*]

Affiliations:

[1] Laboratory of Behavioral Ecology and Evolution, School of Biological Sciences, Seoul National University; Seoul 08826, South Korea

[2] Paleontological Laboratory, School of Earth and Environmental Sciences, Seoul National University; Seoul 08826, South Korea

[3] Makovicky Vertebrate Paleontology Lab, Department of Earth and Environmental Sciences, University of Minnesota; Minneapolis 55455, U.S.A.

[4] Laboratory of Robotics and Intelligent System Engineering, Department of Mechanical Engineering, Sungkyunkwan University; Suwon 16419, South Korea

[5] Laboratory of Integrative Animal Ecology, Department of New Biology, DGIST; Daegu 42988, South Korea

[6] Museum and Institute of Zoology, Polish Academy of Sciences; Wilcza 64, Warsaw, Poland

*Correspondence to:

Correspondence regarding robot design should be addressed to hyungpil@g.skku.edu (HM), regarding paleontological issues should be addressed to ynlee@snu.ac.kr (YL), regarding avian flush-pursuers and their prey should be addressed to sangim@dgist.ac.kr (SL) or piotrjab@behecolpiotrsangim.org (PGJ)

Abstract:

Numerous non-avian dinosaurs possessed pennaceous plumage in the proto-wing and tail[1], whose function remains unclear. We hypothesize that they might have been used during hunting that resembles avian flush-pursuers, who use wing/tail displays to flush hidden prey and pursue it[2,3]. Using a dinosaur robot, we confirmed that efficiency in flushing grasshoppers by moving forelimbs and tail increased when proto-wings were present, especially distally and with contrasting pattern, and when caudal plumage (tail feathers), especially of large surface, was present. Responses of grasshopper escape neurons to animations of distal proto-wing displays matched the observed escape behavior. Hence, the surface of stiff pennaceous feathers might have evolved to exploit the sensitivity of prey escape pathways and to help dinosaurs aerodynamically in quick maneuvers during pursuits after prey.

Main

Spectacular dinosaur fossils with diverse feather types have been discovered in the past three decades[1]. The type of feathers used for flying in modern birds, the pennaceous feathers, are limited to Pennaraptora among dinosaurs[4]. The earliest pennaceous feathers were present on distal forelimbs as small 'proto-wings' and around the tip of the tail as distal caudal plumage in the early-diverging pennaraptorans, as preserved in *Caudipteryx*[5]. Multiple lineages of feathered dinosaurs reached powered flight before the true Aves[6], but the early proto-wings were too small to be used for powered flight[7]. The functions of distal proto-wings and caudal plumage might have been related to foraging/hunting [insect netting[8,9]; pouncing on prey[10]; leaping for prey[11]; immobilizing large prey[12]; running while flapping[13,14]], or other behaviors [brooding[15]; wing-assisted incline running[16]; gliding[17]; intraspecific displays[18,19]] (Supplementary Table 1). Concerted association of multiple inter-related functions might have initiated the evolution of true powered flight in certain ecological context such as foraging and/or predation. Here we propose that a previously overlooked potential function of feathered proto-wings and tail might have played an important role in these evolutionary processes: the function of flushing the prey in the flush-pursue foraging known in extant birds[2,20,21].

Flush-pursue foraging involves displays of contrasting plumage on spread/flicked wings and tails (Fig. 1a–f; Supplementary Note 1). In response to these displays, the prey escape from their hiding places and become available for pursuits (aerial or cursorial) and subsequent captures by predators[2,3]. This strategy exploits the properties of relatively simple neural circuits that mediate prey escape responses to visual stimuli[2,20–22]. This exploitation occurs especially when the prey has difficulty in quickly evaluating the absolute distance to, and the absolute size, speed, and type of, the approaching predator[21]. Visual displays by flush-pursuing birds are found in various families of primarily insectivorous or omnivorous birds (Fig. 1a–g; Extended Data Fig. 1;

Supplementary Notes 1 and 2). The escape behaviors occur in many prey animals[22]: orthopterans[23], flies[24], crabs[25], crayfish[26], and small mammals[27] – taxa that pennaraptoran dinosaurs likely also hunted[28]. Hence, this foraging strategy might also have been used by the small predatory pennaraptorans with widely accepted fast-pursuit predation.

Here, we propose a *Flush-pursue Hypothesis* (Supplementary Table 1; Supplementary Note 3) that includes some of the earlier hypotheses and observed evolutionary trends. It involves three consecutive elements, two of which are shared with other hypotheses: (element 1) visual flush-displays with feathered forelimbs/tails; (element 2) use of feathered forelimbs/tails in drag and/or lift generation for pursues after prey [e.g., the "running while flapping" hypothesis[13,14], the "leaping" hypothesis[11]] or in attacks on flushed prey immediately after it lands on a substrate [similar to "pouncing" hypothesis[10]]; (element 3) use of quick forward moves of head on a long neck as extant birds do, or possibly the use of hindlimbs (or even forelimbs) to capture the prey, which could be aided by the use of proto-wings as insect nets[9] or to immobilize the prey[12]. The hypothesis highlights positive feedback between the "flush (element 1)" and the "pursue-attack (elements 2 and 3)" of the strategy. The use of plumage to flush prey increases the frequency of chases after escaping prey, which in turn increases the importance of plumage in drag-based or lift-based maneuvering for a successful pursuit, leading to an increase in the plumage area and stiffness and the forelimb ability to perform fast movements, which in turn may increase the strength of the visual stimulus in flush-displays, leading to foraging that is even more based on flushing, pursuing and capturing the flushed prey (Supplementary Table 1).

The flush-displays that cause an increase of the frequency and/or the distance at which the prey initiates escapes invariably lead to increased foraging efficiency by avian flush-pursuers[2,20,21]. Hence, the flush-pursue hypothesis can be experimentally evaluated by testing the "flush" function of the distal proto-wings, distal caudal plumage, and their contrasting coloration

on the escape reactions of prey organisms. We used a robot (Robopteryx; Fig. 1h; Methods part 2; Extended Data Figs. 2–4) based on the morphology and size of *Caudipteryx* (Methods parts 1–3) to flush grasshoppers *Oedaleus infernalis* (Fig. 1j; Methods part 4) by visual displays (Fig. 2a; Extended Data Figs. 5–7). The Robopteryx represents a general cursorial bipedal theropod with a long tail and forelimb movement range similar to the early pennaraptoran dinosaurs (Fig. 1h,i). We also recorded responses of the LGMD/DCMD neural pathway (Fig. 1k) involved in orthopterans' visually evoked escape reactions (Methods part 6).

The presence of distal proto-wings increased the flush frequency and the distance at which the prey escaped (Fig. 2b; Supplementary Table 2, Methods part 4: exp. 1). Grasshoppers were flushed more frequently by the distally rather than proximally located proto-wings (Fig. 2c; Supplementary Table 3; Methods part 4: exp. 2). They escaped not only at the spreading stage of the flushing movement (Supplementary Video 1) but also at the folding stage (Supplementary Video 2): in separate tests at 35 cm to the animal, only 35% (7 out of 20) of grasshoppers escaped in response to the forelimb folding movements, while 90% (27 out of 30) of grasshoppers escaped in response to the whole flush-display. Grasshoppers escaped more often when white patches were present on the proto-wings (Fig. 2d; Supplementary Table 4; Methods part 4: exp.3). The flushing performance was higher when caudal plumage was present on the tail (Fig. 2e; Supplementary Table 5; Methods part 4: exp. 4), and when its surface area was larger (Fig. 2e; Supplementary Table 5; Supplementary Video 3). Grasshopper neurons (Fig. 1k) mediating the escape responded more strongly when the distal proto-wings (Supplementary Video 4) were present compared to when they were absent (Fig. 2g; Extended Data Fig. 8a; Supplementary Video 5) in the computer animations of dinosaur forelimb's displays (Fig. 2f; Methods part 6): the firing rate followed the pattern of the angular speed of forelimb movements (Extended Data Fig. 8a). In summary, all the results are consistent with the idea that the proto-

wings, especially distally located and with contrasting patterns, as well as the feathered tails in predatory dinosaurs, might have been used to exploit escapes in their prey in a manner similar to avian flush-pursuers[2,20,21].

The *Flush-pursue Hypothesis* offers a new perspective on the evolution of the pennaceous feathers suggesting that the exploitation of simple neural pathways mediating escape behaviors of prey might have shaped not only the ancestral origins of the avian wing and tail but also some other major evolutionary transitions. We hypothesize that even the earlier theropods (e.g., Compsognathidae) with plumulaceous, filamentous feathers, membranes, and/or color patterns on the tail [e.g., *Sinosauropteryx*[29]] might have used these structures to flush prey. Additionally, hypothetical dinosaurian flush-pursuers might have benefited from the development of the inner ear[30], which might have helped in the precise control of fast motions during pursuit-attacks. Body miniaturization[31] might have helped in fast maneuvers during pursuits and might have been linked to the evolution of insectivory, which is also typical for the extant flush-pursuers. We also hypothesize that the flush-pursue foraging might have contributed to the early evolution of membranous wings in Pterosauromorpha (pending fossil discoveries of pterosauromorphs with proto-wings) as the laterally facing glenoids in Pterosauria and some of their closest precursors Lagerpetidae support the wide range of forelimb motion needed for flush-displays[32].

Methods

Part 1. Selection of *Caudipteryx* as a model for building a robot

We examined the following *Caudipteryx* specimens in publications: *C. zoui* [NGMC 97-4-A (holotype) and NGMC 97-9-A (paratype) of Ji et al. [5]; BPM 0001 of Zhou et al.[33]; PMOL AD00020 of Li et al.[34]], *C. dongi* [IVPP V 12344 (holotype) of Zhou and Wang[35]], *C.* sp. [IVPP V 12430 of Zhou et al.[33]; LPM0005 of Feduccia and Czerkas[36]].

Pennaceous feathers with rachis structure are restricted only to Pennaraptora [Oviraptorosauria + Paraves[4]]. Therefore, the evolution of wings that can be used for aerial locomotion has occurred within this clade. Oviraptorosauria is the phylogenetically most basal clade in Pennaraptora.

We selected the forelimbs of oviraptorosaur *Caudipteryx* as a representation of the ancestral condition of Pennaraptora because *Caudipteryx* is one of the basal taxa with almost completely preserved 'proto-wings'[37]. *Caudipteryx* forelimb and tail pennaceous feathers (open-vaned, broad, and 'frond' shaped) are symmetrical and highly simplified compared to those of flying birds, both extant and extinct[5,38,39]. The pennaceous forelimb feathers of *Caudipteryx* are located distally, and the pennaceous tail feathers are restricted to the tail tip[5,37,39,40]. Although the tail feathers are pennaceous (vaned), no specimen preserves evidence of hooklets on the barbules[5]. In *Caudipteryx* (IVPP V22606), two layers of tail feathers are evident: one layer of shorter rachis-less body feathers and another layer of longer pennaceous tail feathers[41].

The feathered forelimbs of *Caudipteryx* could have produced weak aerodynamic forces in rapid terrestrial locomotion[42]. However, feathers on the forelimbs and tail of *Caudipteryx* are probably not related to flight because they have no striking aerodynamic features and no

150 osteological features to support any aerial capability[38]. Other functions, such as maintaining
151 balance or producing additional thrust during running or climbing, insulating eggs, and
152 displaying, are all viable hypotheses[38]. *Caudipteryx*, with the center of mass situated anteriorly,
153 probably used a running mechanism more similar to that of modern cursorial birds than more
154 basal bipedal dinosaurs[43].

155 The evolution of predator's plumage that visually contrasts with the background appeared to
156 be advantageous in flush-pursuit foraging[44], and light patches on the darker plumage were also
157 shown to be advantageous in the context of flush-pursue foraging[44]. Considering that both the
158 tail and body feathers of *Caudipteryx* are known to be black[34], and visible banding patterns are
159 shown in the tail feathers (striped caudal plumage)[5,45], *Caudipteryx* is a reasonable model species
160 for evaluating the effect of the color pattern of proto-wings/caudal plumage on flushing
161 performance in non-avian dinosaurs.

162 This decision should be viewed in light of the following remarks: (i) *Caudipteryx* is from the
163 early Cretaceous (Barremian-Aptian), whereas the first pennaraptorans are thought to have
164 emerged as late as the middle Jurassic, as evidenced by the more derived *Archeopteryx*[46].
165 However, to infer the ancestral state of the most basal pennaraptorans, using basal taxa rather
166 than the oldest taxa is likely more reliable, pending the discovery of Jurassic caudipterids. (ii) the
167 preservation of gastroliths in several *Caudipteryx* fossils[5,47] indicates that the diet might have
168 included hard plant materials[28]. However, gastroliths may also indicate a diet of arthropods with
169 hard exoskeletons [suggested in extant lizards[48,49]], suggesting an omnivorous diet. In general,
170 the most basal Pennaraptora, Oviraptorosauria, and the derived Paravian theropods,
171 Deinonychosauria, showed a diversity of feeding ecology, including carnivory, insectivory,
172 omnivory, and herbivory[28], a situation similar to the extant avian flush-pursuers [e.g.,[50–52]], for
173 which the flush-pursue strategy is one of many employed during foraging. (iii) *Caudipteryx*

shows particularly short arms and tails[19,53] with a reduced third finger, all of which are derived condition in Oviraptorosauria [the most basal clade of pennaraptoran dinosaurs[19]]. Thus, if the experimentally imitated flush-displays by the relatively short-armed robot generally similar to *Caudipteryx*[19,53] or *Incisivosaurus* [specimens[55] formerly referred to as *Similicaudipteryx*[1]]} will prove efficient in flushing arthropods, then this function will likely be amplified in other relatively long-armed taxa. The flushing function could be easily generalized to other basal pennaraptoran with longer forelimbs such as *Protarchaeopteryx*[5] and Scansoriopterygids[56]. (iv) the arms of many small-bodied theropod dinosaurs, even those believed to have predatory habits, were relatively short and might not have been used at the capture stage, when capture in the mouth with a long and robust neck might have been more efficient[57]. However, the forelimbs equipped with claws could have been used to handle the prey after the capture. (v) *Caudipteryx* shows some disparity in feather size and distribution among caudipterids: pennaceous feathers are more restricted to the distal portion of the forelimb (with shorter secondary feathers) and tail in *Caudipteryx* than in other members of Caudipteridae {e.g., *Incisivosaurus* ["*Similicaudipteryx*"[55]] and *Xingtianosaurus*}. However, since the *Caudipteryx* specimens offer the most complete and comprehensive data among caudipterids and possess the relatively distal distribution of pennaceous feathers on forelimbs and tail (likely to boost the efficiency in flush-pursuit foraging), we think that the use of *Caudipteryx* with its distal proto-wings as a model ancestral early-diverging pennaraptoran is both conservative and represents the best use of the available data.

Since its initial report in 1998, *Caudipteryx* still serves as the most representative basal-most pennaraptoran in the fossil record currently known, and we aim to shed light on the evolution of proto-wings and caudal plumage considering the following assumptions:

(i) the early members of Pennaraptora generally had similar proto-wings' dimensions (relative to body size) to those of *Caudipteryx* and

(ii) their forelimb's movement range was anatomically restricted in a manner similar to *Caudipteryx*;

(iii) the early members of Pennaraptora hunted small prey such as insects, crustaceans (e.g., crabs), small reptiles, and small mammals that use visually triggered escape behaviors to avoid predation;

(iv) the early members of Pennaraptora were skilled in chasing (running) the flushed prey.

Part 2. Building a robot based on the morphology and size of *Caudipteryx*

Based on the skeletal and plumage anatomy of fossil specimens of *Caudipteryx*, we built a robot (Robopteryx; Fig. 1h; Extended Data Fig. 2a) of a size similar to that of *Caudipteryx*. Of the known *Caudipteryx* specimens, we chose IVPP 12430[33] for the overall body proportions (length of body, hip height, length of arms, and tail), IVPP 12344[35] for the shape of the proto-wing, and NGMC 97-4-A for the tail feather dimensions and pattern[5], and PMOL AD00020 for coloration[34]. The dimensions of arms and proto-wing referred to the identical specimens as in Talori et al.[13]. There is an indication that the presence of propatagium should be treated tentatively[58]. However, based on the visible contour of what is presumed to be the propatagium and as inferred from the preserved positions of the forelimbs, we imitated the propatagium based on LPM0005[36].

As the tail feathers of reported *Caudipteryx* specimens are folded in half, the opened outline was inferred from the tail fan of *Incisivosaurus* STM22-6[1] (formerly known as a specimen of *Similicaudipteryx*). We took a conservative approach and assumed the folded tail feathers of (PMOL AD00020) represented the anteriormost margin of the opened tail fan and assumed that

222 the distal-most feathers would have filled in the gap of the fan, as in STM22-6, to form a
223 continuous fan.
224 The robot was built from aluminum (A6061); the CAD used to build the robot is shown in
225 Extended Data Fig. 3a,b. We made proto-wings and caudal plumage using black-colored paper
226 (Fig. 2a). Plastic pieces were inserted between segments of the proto-wing to control their
227 minimum and maximum range of movements (Extended Fig. 2d1–d3). The propatagium was
228 made of black elastic stocking (Extended Data Fig. 2b), and the head was built using black-
229 colored polystyrene (Fig. 1h; Extended Data Fig. 2a). For imitating a bent tail, an additional
230 structure was attached to the tail part (Extended Data Fig. 2c). The main body was covered with
231 black-colored felt (Fig. 1h; Extended Data Fig. 2a).
232 The tendon-driven mechanism was applied to the robot's forelimb and tail motions. Fishing
233 line (thickness: 0.47 mm, tensile strength: 45 kg) or belt were used as tendons (Extended Data
234 Fig. 3c1–d2), which were each connected to a motor (XM430-W210-R, Robotis), respectively.
235 For the forelimb motion, two fishing lines were used in controlling motion for the pitch and yaw
236 rotation (green and blue lines in Extended Data Fig. 3c1,c2); a belt was used in controlling
237 motion for the roll rotation (red line in Extended Data Fig. 3c1,c2). The fishing line controlling
238 the yaw axis was also designed to also rotate the elbow joint. An additional fishing line (yellow
239 line in Extended Data Fig. 3c1,c2) was used in rotating the wrist joint passively. For the tail
240 motion, a motor with a fishing line was used to control the pitch rotation (green line in Extended
241 Data Fig. 3d1,d2). Additionally, we implemented the yaw motion (motor no.5 in Extended Data
242 Fig. 3d1,d2) and spread the tip of the tail (blue line in Extended Data Fig. 3d1,d2) in the robot.
243 The schematic diagram of the robot control system is shown in Extended Data Fig. 3e. The
244 robot controller (OpenCM9.04-C, Robotis) receives an operation command created from a
245 mobile phone through the Bluetooth communicator (BT-410, Robotis). The controller is

connected to a series of nine motors, and the power is supplied through an external battery (LIPO Battery LB-020, Robotis) directly connected to one of the motors.

Part 3. Choosing the postures and movements of the forelimbs and tail

We needed to set the range of angular movements performed by the robot's forelimb and tail to imitate the hypothetical ranges of *Caudipteryx*. We considered several angle types in the robot (Extended Data Fig. 4) as descried below:

Angles defined in the side view of the robot (Extended Data Fig. 4a, upper row):

- Shoulder angle (S) – The angle between the humerus structure and a horizontal line parallel to the lower part of the main body.
- Elbow angle (E) – The joint angle at the elbow.
- Wrist angle (W) – The joint angle at the wrist.
- Tail angle (T) – The angle between the tail structure and the main body.

Angles defined in the frontal view (Extended Data Fig. 4b, lower row):

- Lift angle (L) – The angle between the humerus structure and the vertical line running along the side of the main body.

Based on the literature[59], the angles should ideally be set to the following values at the resting posture: ~33° for S, ~106° for E, and ~131° for W. However, due to the limit in the robot's design (one motor controls the two joints), we always set values of the E and W to be identical: ~106°. This setting allows mimicking the spreading and folding of the arm as a consequence of

automatic wrist folding[60]. The automatic wrist folding mechanism was previously known from volant birds[60] but was recently also described in alligators and ostriches[61]. Therefore, by the extant phylogenetic bracketing approach[62] and the presence of propatagium[36], *Caudipteryx* is expected to have used a similar mechanism, as has been proposed even for *Chilesaurus*[63] of debated affinity inside Dinosauria[64–66]. Hence, we set the values for the resting posture in the S, E, and W as 33°, 106°, and 106°, respectively (Extended Data Fig. 4a). We set the angle L as 12°, a consequence of the robot's forelimb structure (Extended Data Fig. 4a).

Estimating the range of motion helps infer joint mobility *in vivo*[61]. Because the exact range of motion cannot be directly induced from the bones of *Caudipteryx*, as the bones are all compressed during taphonomic processes in known specimens, we used a conservative method of phylogenetic bracketing. In this method, we chose model organisms representing a more basal condition (*Acrocanthosaurus*) and a more derived condition (*Bambiraptor*)[67] and assumed that the range of motion at the shoulder joint of *Caudipteryx* would have been in between those two. In other words, the data for the two taxa offer estimates of the minimum and maximum range of motion (Supplementary Table 8) in the phylogenetically intermediate taxon of our interest. Morphology of the articular surface of the glenoid, where the upper arm (humerus) meets the shoulder (scapula), of *Caudipteryx* specimens, indicates that they were unlikely to have been held over horizontally [Senter[67], *contra* Talori et al.[13]], or have had a range of motion seen in more derived dromaeosaurids, much less than in birds. The range of motion in shoulder raising may have been closer to *Acrocanthosaurus* [68], which probably could not be raised to the horizontal[69]. The elbow flexion is beyond 90 degrees in Ornithomimosauria and more derived clades[70]. The range of motion in the elbow might be intermediate between *Acrocanthosaurus* and *Bambiraptor*, with its folding movements closer to *Bambiraptor*[69]. As for the wrist, the radial angles of *Caudipteryx* imply that the range of abduction was even greater than in

dromaeosaurids[71]. Therefore, we assumed that the wrist could fold like some extant birds but could not be held straight[71]. In summary, we used the following estimated motion ranges: 19°~2° ≤ S ≤ 114°~123°, 55° ≤ E ≤ 136°, 0° ≤ W < 180°, L ≤ 88° (Supplementary Table 8).

We chose a hypothetical forelimbs' flushing movement within the estimated motion range (Supplementary Video 6). The proto-wings' flushing movement (Extended Data Figs. 4a and 5) started from the resting posture (S = 33°, E = 106°, W = 106°, L = 12°) to the estimated maximum value of each angle (S = 123°, E = 136°, W = 136°, L = 88°; this process takes 0.42 sec), pause for 0.2 sec, and then revert to the resting posture (this process takes 0.42 sec). This movement shows very similar forelimbs' trajectory to the ground-foraging flush-pursuers [e.g., Greater Roadrunner (*Geococcyx californianus*; link 1 provided in Supplementary Note 1), Rufous-tailed Scrub Robin (*Cercotrichas galactotes*; link 25 to 28 provided in Supplementary Note 1)]. The Greater Roadrunner's flushing movement speeds are about 0.23 sec for wing spreading and folding (link 1 provided in Supplementary Note 1).

With a proportionately large body, *M. longissimus* and *M. ilio-ischiocaudalis*, oviraptorosaurs would have been capable of swinging and twisting their tails both mediolaterally and dorsoventrally with a degree of muscular dexterity beyond that of most other theropods and modern reptiles[19]. However, in the robot, we only used a simple vertical up-down tail movement imitating the tail-flushing movement of some of the extant flush-pursuers (Supplementary Note 1): the value of T is from 150° to 90° (this process takes 0.33 sec), and then revert to 150° (this process takes 0.33 sec; Extended Data Figs. 4b and 6). Sidewise movements with the tail, present in some flush-pursuers, were impossible due to the robot's design constraints.

Part 4. Behavioral experiments: responses of grasshopper to the robot's flushing movements

We conducted behavioral experiments on the band-winged grasshopper *Oedaleus infernalis* (Orthoptera), which can serve as a model of prey susceptible to flush-pursue foraging. We chose it as the study species because of its high abundance. Species identification was made using field guide books on Orthoptera[72,73]. As the escape behavior of orthopterans is likely affected by sex[74], we tested adult males only. The sex was identified based on the body shape and size in the field without capturing the animals.

Orthoptera is an ancient prey taxon[75] that evolved a fast escape reaction as an adaptation to avoid attacking predators[75]. The grasshoppers may be unable to precisely evaluate the distance, size, and type of an approaching predator due to constraints of their sensory systems, including relatively poor resolution and close distance between the eyes. Instead, they use relatively simple looming-detect neural circuits that mediate the visually triggered escapes in response to looming objects[76,77], including fast-approaching predators. The visual displays by flush-pursue predators produce those types of stimuli and exploit the visually triggered escape responses in prey.

From August to September 2020 and 2021, we conducted behavioral experiments on males of *Oedaleus infernalis* (Fig. 1j) along a 2-Km-long trail (37°40'12.3"N, 126°53'11.4"E) in Go-yang and a 1-Km-long trail (35°42'00.2"N 128°27'29.0"E) in Dae-gu, South Korea. We chose grasshoppers resting on the road/path where the robot can be easily placed facing the grasshopper without much disturbance. We tested the grasshopper's frequency of escapes in response respond to the robot's movements (see experimental treatment description below). The experiments were conducted according to the following general procedure (e.g., Fig. 1h): (1) Gently place a length-marked wooden stick next to the grasshopper. (2) Take a picture of the grasshopper and record its body orientation relative to the robot's position. (3) Run the robot's forelimb or tail display movements (using phone wireless controller software) at a specific

342 distance(s), depending on the experiment. If the grasshopper escaped at first (the farthest)
343 distance, the experiment on the individual was over. But if the grasshopper did not respond to the
344 robot's movements, we moved the robot to the next test distance closer to the grasshopper until
345 the grasshopper responded or until the closest distance to the grasshopper planned in the
346 experimental design. To place the robot in front of the grasshopper, we moved the robot
347 carefully using a long beam attached to the robot. We tested 3 to 5 individuals in one
348 experimental treatment, followed by 3-5 tests in the subsequent treatment, and some experiments
349 with the third experimental treatment; finally, we tested 3-5 individuals in the third treatment,
350 after which we returned to using the first treatment. We repeated this cycle for several hours per
351 day, resulting in no bias among treatments regarding the time of day. To avoid the possible effect
352 of the shadow created by the robot's movements on the grasshopper's response, we placed the
353 robot where no shadows would appear near the grasshopper while the robot's forelimbs or tail
354 were moving. The main body of the robot was tilted 37° upward for the experiments concerning
355 the proto-wings (experiments 1 to 3; Extended Data Fig. 2e) to imitate a posture observed in
356 ground flush-pursuers that use wing displays such as greater roadrunners, northern mockingbirds,
357 or rufous-tailed scrub robins (see Supplementary Note 1). The main body of the robot was tiled
358 40° downward for an experiment concerning caudal plumage (experiment 4; Extended Data Fig.
359 2f) to imitate a situation of a body tilted forward during tail displays in some of the flush-
360 pursuers such as in the body pivoting of *Myiobrous* redstarts with upward-lifted and spread tail,
361 or similar to the willie wagtail's (*Rhipidura leucophrys*) foraging movements at short moments
362 when the tail is quickly cocked upwards while the head points downward.
363
364 **Experiment 1. The effect of the presence of proto-wings on the forelimbs and the motor**
365 **sound created during the robots' flushing movement on the flushing performance.**

We used three experimental conditions: (1-1) robot presented without forelimb movements but with sounds of the robot played back through a speaker (Extended Data Fig. 7a1); (1-2) movements of forelimbs without proto-wings (Extended Data Fig. 7a2); (1-3) movements of forelimbs with distal proto-wings (Extended Data Fig. 7a3). Since auditory cues are also used to detect predators[74], condition (1-1) was used to determine the effect of noise that occurs when the robot is operating. The motor noise was recorded using a microphone (BY-MM1, BOYA) connected to a smartphone before the experiments, and it was played through a speaker (XMYX03YM, Xiaomi) attached to a structure between the legs of the robot. The test distances were 100, 80, 60, 40, and 20 cm (between the grasshopper and the point between the robot wheels). We found that grasshoppers were not seriously affected by the motor sound (only two jumped away out of total 46 tests in the 1-1 condition) and that the remaining treatments with moving forelimbs triggered escapes significantly more often than the sound-only treatment: Dunn's test with Bonferroni correction, P for (1-1) vs. (1-2) < 0.001, (1-1) vs. (1-3) < 0.0001 (Extended Data Fig. 9; Supplementary Table 2). Based on these comparisons, we regarded the sound effect on grasshoppers' escapes as negligible, and we focused on the comparisons between the two remaining treatments (i.e., 1-2 vs. 1-3) presented in the main text Fig. 1b.

Experiment 2. **The effect of the presence and location of proto-wings on the flushing performance.**

For efficient gliding, the development of surfaces near the body is expected[10]. For efficient flushing and pursuing the prey, by contrast, the development of surfaces on the distal parts of the forelimbs is expected because it produces a relatively stronger visual stimulus during limb movements. To determine the effect of the presence and location of the proto-wings on the flushing performance, we tested grasshoppers in three experimental treatments: (2-1) proto-

wings absent (Extended Data Fig. 7b1); (2-2) proximal proto-wings present (Extended Data Fig. 7b2); (2-3), and distal proto-wings present (Extended Data Fig. 7b3). Proximal and distal proto-wings have an identical surface area (128 cm^2) to the distal proto-wings at the peak of the visual stimulus of the flushing movement (right before folding the forelimbs). Based on the results of Experiment 1, we chose 70 and 35 cm as test distances to simplify the experimental procedure in Experiment 2. None of the grasshoppers responded to the robot's flushing movement at 70 cm. Therefore, we only used the responses at 35 cm for statistical comparisons among the treatments. We also noticed that the grasshoppers escaped at the forelimbs' spreading stage as well as folding stage of the flushing movement. We thus conducted an additional experiment to compare the effect of opening-only *vs.* folding-only movement on the grasshoppers' escapes at 35 cm to the grasshopper.

Experiment 3. The effect of proto-wings' color contrast on the flushing performance.

Plumage color patterns in non-avian feathered dinosaurs might have played a role in many aspects of their life, including signaling function, thermoregulation, and crypsis[18,78,79]. Plumage coloration, such as the light and dark regions in the tail fan of *Caudipteryx*[5], might have been used in display and communication (e.g., intersexual communication)[18,19,80,81] regardless of whether it was used for flush-pursuing or not. For example, some extant flush-pursuers, such as the Painted redstart (*Myioborus pictus*), use white patches in flushing the prey[82] as well as in territorial interactions (the display behavior is different from these two functions). Hence, similar situations might have occurred among the pennaraptoran dinosaurs. The contrast in the plumage is known to affect the foraging efficiency of extant flush-pursuers [e.g., [2,20,21]]. To determine the effect of proto-wings' color contrast on flushing performance, we tested grasshoppers in two experimental treatments: (3-1) plain black proto-wings (Extended Data Fig. 7c1); (3-2) white-

patched proto-wings (Extended Data Fig. 7c2). Using white paint, we created a hypothetical stripe pattern (Extended Data Fig. 7c3) on the original black proto-wings. As none of the grasshoppers escaped at the distance of 70 cm in Experiment 2, we chose closer distances: 60 and 50 cm. Also, considering that 90% of grasshoppers escaped in response to the robot's flushing movement equipped with the proto-wings in Experiment 2 at 35 cm, we chose a slightly larger distance of 40 cm as the nearest distance to be able to observe differences between the plain black proto-wings and the white-patched proto-wings treatments in the frequency of escapes. Hence, in Experiment 3, we used three subsequent distances in the field procedure: 60, 50, and 40 cm. As the grasshoppers escaped only at the distance of 40 cm, the statistical comparison between the two treatments was conducted only on the results from 40 cm tests.

Experiment 4. The effect of the presence and area of caudal plumage on the flushing performance.

We tested grasshoppers in three experimental treatments: (4-1) caudal plumage absent (Extended Data Fig. 7d1); (4-2) normal-sized caudal plumage present (Extended Data Fig. 7d2; 262 cm^2); (4-3) large-sized caudal plumage present (twice the surface area of 4-2; Extended Data Fig. 7d3; 524 cm^2). The effect of upward tail movements (the only type possible to imitate with our robot) can only be expected with the tail is not blocked by the head, neck, and body of the dinosaur/robot. Therefore, we imitated a hypothetical situation when the predator already focuses on the ground and has its head down and body tilted downward (Extended Data Fig. 2f). We used 80 and 60 cm from the robot, which resulted in much closer distances to the immobile downward tilted head (the distance between the head and the grasshopper was 10 and 30 cm, respectively).

438 **Part 5. Statistical analyses**

439

440 All statistical analyses were conducted in R version 4.0.3[83]. The Dunn's test with Bonferroni
441 correction was used to determine the differences in the flushing performance in multiple pairwise
442 comparisons using "dunn.test" function in dunn.test package[84] for Experiments 1 and 4. For
443 Experiments 1 and 4, the distance at which the grasshopper escaped [e.g., 100, 80, 60, 40, 20, 0
444 (= "no response") in Experiment 1] was used as the dependent variable. The experimental
445 treatment was used as the independent variable.

446 In Experiment 2, the Chi-square test with Bonferroni correction was performed to determine
447 the differences in the flushing frequency between the experimental treatments using the
448 "pairwiseNominalIndependence" function in rcompanion package[85]. In Experiment 3, the Chi-
449 square test with Yates' continuity correction was performed to determine the differences in the
450 flushing performance between the experimental treatments using the "chisq.test" function in stats
451 package[83]. For Experiments 2 and 3, the grasshopper's escape behavior (binary variable: escaped
452 or not) was used as the dependent variable, and the experimental treatment was used as the
453 independent variable.

454 Data points in the cases when the grasshopper escaped while moving the robot between
455 distances and before the robot displayed were excluded from the statistical analyses. Given that
456 we repeatedly switched experimental conditions during the day, the effect of the temperature was
457 not addressed in the statistical analyses. During the experiments, we could not control the
458 grasshopper's body orientation, relative to the robot's position. The pattern of escape neurons'
459 firing activity may vary depending on the eye region that faces the display[86], and the frontal
460 approach of a visual stimulus shows a different escape pattern from the other approach directions
461 [from the side and back[87]]. Therefore, we conducted two statistical analyses: one using all the

462 data and another using the smaller data set after removing the data points from the tests when the
463 robot was placed in front or behind the grasshopper. Analyses of both data sets led to the same
464 conclusions. The statistical significance of the effects tested in the experiments is presented as
465 asterisks in the main text, while the detailed information is given in the captions to
466 Supplementary Tables 2 to 5.
467
468 **Part 6. Extracellular neurophysiological recordings from grasshopper's LGMD/DCMD**
469 **pathway**
470
471 **Animations**
472 Similar to the *Caudipteryx* robot (Robopteryx) used in the behavioral experiments, we created
473 *Caudipteryx* animations based on the morphology and size of *Caudipteryx* specimens (see
474 Methods part 2 for specimen information) using a 3D animation software: Blender (version
475 3.2.0). Those animations imitate the dinosaur, similar to the robot, except for the neck and head,
476 which are more naturalistically imitated in the animation. In the animations, like in the
477 Robopteryx, the hypothetical dinosaurian flush-pursuer moves its forelimbs from the estimated
478 resting posture (S = 33°, E = 106°, W = 106°, L = 4°) to the estimated maximum value of each
479 angle (S = 123°, E = 136°, W = 178°, L = 88°; this process takes 0.23 sec), pause for 0.1 sec, and
480 then reverts to the forelimbs' resting posture along the same trajectory as the expansion
481 trajectory (this process takes 0.23 sec; see Methods part 3 for estimated motion range
482 information). We produced two animations of the forelimb-flushing dinosaur without and with
483 distal proto-wings (Supplementary Videos 4 and 5).
484 We also produced an animation of a simple looming stimulus (an approaching circle; $l/|v| = 5$
485 ms, where l is the radius of 3 cm and v is the imitated constant approaching speed of 6 m/s;

Supplementary Video 7) similar to the classical stimuli that have been used over more than 45 years of classical neurophysiological studies of the LGMD/DCMD pathway and are exemplified by several influential classical reports[88–92]. In the animations, the dinosaur and circle are colored black (R – 000, G – 000, B – 000), and the background is colored light gray (R – 203, G – 203, B – 203). Since we placed the grasshopper ventral side up in the experiments, the hypothetical dinosaurian flush-pursuer was oriented upside down in the animations (Extended Data Fig. 10b).

Study subjects

We used adult males of the band-winged grasshopper *Oedaleus infernalis* collected from the study sites where the behavioral experiments were conducted. We kept them in an indoor breeding facility and fed them with grasses.

Laboratory set-up

In the lab, we used tape to fix a grasshopper's ventral side up onto a cork board (Extended Data Fig. 10a–c). We removed the antennae to prevent noise and prevent accidental obstruction of the view. Then, we slightly tilted the head backward using a pin to expose the neck connectives (between the head and thorax). Beeswax was added to both sides of the neck to keep the saline solution in there. One eye (the left one) was covered with beeswax to block the view. Next, we carefully dissected the soft ventral part of the neck to expose the ventral nerve cords (Extended Data Fig. 10d). We dropped the saline solution (NaCl 210 mM, KCl 7.1 mM, $CaCl_2$ 9.0 mM, Tris-buffered to pH 6.8) on the part and hooked an extracellular silver wire electrode (127-µm bare diameter, AM systems) to the contralateral nerve cord (Extended Data Fig. 10e,f). The other wire of the electrode with a pin is pinned on the abdomen (Extended Data Fig. 10c). We used a stereoscope during dissecting and placing the electrode. The electrode was attached to an

electrode holder (H-13, Narishige), and the holder was manipulated using Micromanipulator (MM-3, Narishige). The electrode was connected to the Neuron SpikerBox Pro (Backyard Brains, USA), which was connected to a laptop. The BYB Spike recorder (Backyard Brains, USA) was used in the laptop to record neural activity in response to *Caudipteryx* animations at the 10 kHz sampling rate. During the recording from the nerve cord, the BYB Spike recorder shows DCMD spikes in real-time. To synchronize the neural activity and visual stimuli, we recorded a high-speed video using iPhone (12 mini; 240 fps). Animations were projected on a flat-screen monitor (TFG32Q14P IPS QHD 144, Hansung computer; 32 Inch) with a display brightness of 400 cd/m^2 and a refresh rate of 120 Hz. The distance between the monitor and the grasshopper was set to 35 cm (Extended Data Fig. 10a). To reduce the noise in the recordings, we used a separate cable to connect the Neuron SpikerBox Pro, Laptop, and Micromanipulator to the ground.

We confirmed that a black looming circle stimulus ($l/|v|$ = 5 ms) displayed on the monitor triggered the grasshopper's response, known as the typical spiking frequency response to a fast looming stimulus (Extended Data Fig. 8b,c): an accelerating increase in firing rate up to the maximum point after which the rate decreases.

Experimental Design

To determine the effect of the presence of proto-wings on the neural response of the LGMD/DCMD pathway, we compared the responses of grasshoppers to two forelimb animations: (1) display without proto-wings (NoPW treatment); (2) display with distal proto-wings (PW). They were played six times each to each grasshopper in one of the two experimental orders: (PW, NoPW, PW, NoPW, PW, NoPW, PW, NoPW, PW, NoPW, PW, NoPW) or (NoPW, PW, NoPW, PW, NoPW, PW, NoPW, PW, NoPW, PW, NoPW, PW). Additionally, for each individual, we played a looming circle animation (black circle of $l/|v|$ = 5

ms) at the beginning and end of recording neurophysiological responses. A pause of 1 min followed each stimulus presentation. Hence the duration of a set of experiments for each individual was about 20 min.

Analysis

We analyzed the neural spike data using Spike2 software (version 5, Cambridge Electronic Design, Cambridge). We followed numerous previous studies exemplified by several classical studies[88–92] in identifying of DCMD spikes in the recordings based on spike amplitude, general shape, and response pattern. We confirmed that our method results in extracellularly recorded spikes that match the well-known pattern of DCMD responses with respect to the typical spiking frequency response to a fast-looming stimulus (Extended Data Figs. 8b,c).

We first inspected the recorded firing rate with a bin size of 10 ms (Extended Data Fig. 8d), and we realized that even at this relatively narrow bin size, the maximum spiking frequency is almost always observed at the beginning of the display (within the first 10 ms). To analyze the differences in the firing rate profile between the two treatments, we used the wider bin size (25 ms), which produces a more general view of the response better suited for our comparisons and was previously used in some of the classical neurophysiological studies of the LGMD/DCMD pathway [e.g., [89]].

For each frame of the looming circle animation, we determined the angular size subtended by the circle on the retina and calculated the changes in the angular speed of expansion during animation. For each frame in the forelimb animations, we determined the angular distance between the tips of the left and right forelimb (i.e., wing span; proto-wing tips were used for the "with proto-wings" animation), and we used them to calculate the angular speed based on the changes in the angular wing span.

A comprehensive study of the neurophysiological responses to a whole variety of hypothetical displays by flush-pursuing dinosaurs to determine the hypothetically most efficient display movements will be presented separately. The current report clearly illustrates the potential benefits of increased frequency of flushing prey and increased intensity of the DMCD response to one of the typical display movement types known in the extant flush-pursuing birds. A separate comprehensive study will evaluate the full spectrum of different displays by wings and tails known in the extant avian flush-pursuers.

References

1. Xu, X. Filamentous integuments in nonavialan theropods and their kin: advances and future perspectives for understanding the evolution of feathers. in *The evolution of feathers* 67–78 (Springer, Cham, 2020).
2. Jabłoński, P. G. A rare predator exploits prey escape behavior: The role of tail-fanning and plumage contrast in foraging of the painted redstart (*Myioborus pictus*). *Behav. Ecol.* **10**, 7–14 (1999).
3. Remsen, J. V. & Robinson, S. K. A classification scheme for foraging behavior of birds in terrestrial habitat. *Stud. Avian Biol.* **13**, 144–160 (1999).
4. Foth, C., Tischlinger, H. & Rauhut, O. W. M. New specimen of *Archaeopteryx* provides insights into the evolution of pennaceous feathers. *Nature* **511**, 79–82 (2014).
5. Ji, Q., Currie, P. J., Norell, M. A. & Ji, S.-A. Two feathered dinosaurs from northeastern China. *Nature* **393**, 753–761 (1998).
6. Pei, R. *et al.* Potential for powered flight neared by most close avialan relatives, but few crossed its thresholds. *Curr. Biol.* **30**, 4033-4046.e8 (2020).
7. Dececchi, T. A., Larsson, H. C. E. & Habib, M. B. The wings before the bird: An evaluation of flapping-based locomotory hypotheses in bird antecedents. *PeerJ* **2016**, (2016).
8. Ostrom, J. H. Bird flight: How did it begin? *Am. Sci.* **67**, 46–56 (1979).
9. Ostrom, J. H. Archaeopteryx and the origin of flight. *Q. Rev. Biol.* **49**, 27–47 (1974).
10. Garner, J. P., Taylor, G. K. & Thomas, A. L. R. On the origins of birds: The sequence of character acquisition in the evolution of avian flight. *Proc. R. Soc. B Biol. Sci.* **266**, 1259–1266 (1999).

11. Caple, G., Balda, R. P. & Willis, W. R. The physics of leaping animals and the evolution of preflight. *Am. Nat.* **121**, 455–476 (1983).
12. Fowler, D. W., Freedman, E. A., Scannella, J. B. & Kambic, R. E. The predatory ecology of *Deinonychus* and the origin of flapping in birds. *PLoS One* **6**, (2011).
13. Talori, Y. S. *et al.* Winged forelimbs of the small theropod dinosaur *Caudipteryx* could have generated small aerodynamic forces during rapid terrestrial locomotion. *Sci. Rep.* **8**, 1–14 (2018).
14. Zhao, J. *et al.* Reconstruction of *Caudipteryx* robot to identify the origin of avian flapping flight. *Proc. Inst. Mech. Eng. Part C J. Mech. Eng. Sci.* **236**, 8358–8366 (2022).
15. Hopp, T. P. & Orsen, M. J. Dinosaur Brooding Behavior and the Origin of Flight Feathers. in *Feathered Dragons* 234–250 (Indiana University Press, 2004).
16. Dial, K. P. Wing-assisted incline running and the evolution of flight. *Science* **299**, 402–404 (2003).
17. Norberg, U. M. Evolution of vertebrate flight: An aerodynamic model for the transition from gliding to active flight. *Am. Nat.* **126**, 303–327 (1985).
18. Li, Q. *et al.* Plumage color patterns of an extinct dinosaur. *Science* **327**, 1369–1372 (2010).
19. Persons, W. S., Currie, P. J. & Norell, M. A. Oviraptorosaur tail forms and functions. *Acta Palaeontol. Pol.* **59**, 553–567 (2014).
20. Mumme, R. L. Scare tactics in a neotropical warbler: White tail feathers enhance flush-pursuit foraging performance in the slate-throated redstart (*Myioborus miniatus*). *Auk* **119**, 1024–1035 (2002).
21. Jabłoński, P. G. & Strausfeld, N. J. Exploitation of an ancient escape circuit by an avian predator: Relationships between taxon-specific prey escape circuits and the sensitivity to visual cues from the predator. *Brain. Behav. Evol.* **58**, 218–240 (2001).

22. Peek, M. Y. & Card, G. M. Comparative approaches to escape. *Curr. Opin. Neurobiol.* **41**, 167–173 (2016).

23. Gabbiani, F., Krapp, H. G., Koch, C. & Laurent, G. Multiplicative computation in a visual neuron sensitive to looming. *Nature* **420**, 320–324 (2002).

24. Holmqvist, M. H. & Srinivasan, M. V. A visually evoked escape response of the housefly. *J. Comp. Physiol. A* **169**, 451–459 (1991).

25. Oliva, D., Medan, V. & Tomsic, D. Escape behavior and neuronal responses to looming stimuli in the crab *Chasmagnathus granulatus* (Decapoda: Grapsidae). *J. Exp. Biol.* **210**, 865–880 (2007).

26. Schadegg, A. C. & Herberholz, J. Satiation level affects anti-predatory decisions in foraging juvenile crayfish. *J. Comp. Physiol. A Neuroethol. Sensory, Neural, Behav. Physiol.* **203**, 223–232 (2017).

27. Moore, T. Y., Cooper, K. L., Biewener, A. A. & Vasudevan, R. Unpredictability of escape trajectory explains predator evasion ability and microhabitat preference of desert rodents. *Nat. Commun.* **8**, 1–9 (2017).

28. O'Connor, J. K. & Zhou, Z. The evolution of the modern avian digestive system: insights from paravian fossils from the Yanliao and Jehol biotas. *Palaeontology* **63**, 13–27 (2020).

29. Chen, P. J., Dong, Z. M. & Zhen, S. N. An exceptionally well-preserved theropod dinosaur from the Yixian Formation of China. *Nature* **391**, 147–152 (1998).

30. Hanson, M., Hoffman, E. A., Norell, M. A. & Bhullar, B. A. S. The early origin of a birdlike inner ear and the evolution of dinosaurian movement and vocalization. *Science* **372**, 601–609 (2021).

31. Lee, M. S. Y., Cau, A., Naish, D. & Dyke, G. J. Sustained miniaturization and anatomical innovation in the dinosaurian ancestors of birds. *Science* **345**, 562–566 (2014).

637 32. Ezcurra, M. D. *et al.* Enigmatic dinosaur precursors bridge the gap to the origin of
638 Pterosauria. *Nature* **588**, 445–449 (2020).
639 33. Zhou, Z. H., Wang, X. L., Zhang, F. C. & Xu, X. Important features of *Caudipteryx*-
640 evidence from two nearly complete new specimens. *Vertebr. Palasiat.* **38**, 243–265 (2000).
641 34. Li, Q. *et al.* Melanosome evolution indicates a key physiological shift within feathered
642 dinosaurs. *Nature* **507**, 350–353 (2014).
643 35. Zhou, Z. & Wang, X. A new species of *Caudipteryx* from the Yixian Formation of
644 Liaoning, northeast China. *Vertebrata PalAsiatica* vol. 38 111–127 (2000).
645 36. Feduccia, A. & Czerkas, S. A. Testing the neoflightless hypothesis: Propatagium reveals
646 flying ancestry of oviraptorosaurs. *J. Ornithol.* **156**, 1067–1074 (2015).
647 37. Talori, Y. S. *et al.* Identification of avian flapping motion from non-volant winged
648 dinosaurs based on modal effective mass analysis. *PLoS Comput. Biol.* **15**, 1–16 (2019).
649 38. Xu, X. & Guo, Y. The origin and early evolution of feathers: insights from recent
650 paleontological and neontological data. *Vertebr. Palasiat.* **10**, 311–329 (2009).
651 39. Mayr, G. *Avian Evolution*. *Wiley-Blackwell* (2016). doi:10.1002/9781119020677.
652 40. O'Connor, J. K. *et al.* An enantiornithine with a fan-shaped tail, and the evolution of the
653 rectricial complex in early birds. *Curr. Biol.* **26**, 114–119 (2016).
654 41. Wang, W. & O'Connor, J. K. Morphological coevolution of the pygostyle and tail feathers
655 in Early Cretaceous birds. *Vertebr. Palasiat.* **55**, 289–314 (2017).
656 42. Talori, Y. S. & Zhao, J. S. Aerodynamics of soft flapping wings of *Caudipteryx*. *Lect.*
657 *Notes Comput. Sci. (including Subser. Lect. Notes Artif. Intell. Lect. Notes Bioinformatics)*
658 **11742 LNAI**, 155–170 (2019).
659 43. Jones, T. D., Farlow, J. O., Ruben, J. A., Henderson, D. M. & Hillenlus, W. J. Cursoriality
660 in bipedal archosaurs. *Nature* **406**, 716–718 (2000).

661 44. Jabłoński, P. G. & Strausfeld, N. J. Exploitation of an ancient escape circuit by an avian
662 predator: Prey sensitivity to model predator display in the field. *Brain. Behav. Evol.* **56**,
663 94–106 (2000).
664 45. Roy, A., Pittman, M., Saitta, E. T., Kaye, T. G. & Xu, X. Recent advances in amniote
665 palaeocolour reconstruction and a framework for future research. *Biol. Rev.* **95**, 22–50
666 (2020).
667 46. Godefroit, P. *et al.* Reduced plumage and flight ability of a new Jurassic paravian
668 theropod from China. *Nat. Commun.* **4**, 6–11 (2013).
669 47. Wings, O. A review of gastrolith function with implications for fossil vertebrates and a
670 revised classification. *Acta Palaeontol. Pol.* **52**, 1–16 (2007).
671 48. Johnson, D. R. Diet and estimated energy assimilation of three Colorado lizards. *Am. Midl.*
672 *Nat.* **76**, 504–509 (1966).
673 49. Sokol, O. M. . Lithophagy and geophagy in reptiles. *J. Herpetol.* **5**, 69–71 (1971).
674 50. Hughes, J. M. Greater Roadrunner (*Geococcyx californianus*), version 1.0. In Birds of the
675 World (A. F. Poole, Editor). *Cornell Lab of Ornithology, Ithaca, NY, USA* (2020)
676 doi:10.2173/bow.greroa.01.
677 51. Farnsworth, G., Londono, G. A., Martin, J. U., Derrickson, K. C. & Breitwisch, R.
678 Northern Mockingbird (*Mimus polyglottos*), version 1.0. In Birds of the World (A. F.
679 Poole, Editor). *Cornell Lab of Ornithology, Ithaca, NY, USA* (2020)
680 doi:10.2173/bow.normoc.01.
681 52. Collar, N. Rufous-tailed Scrub-Robin (*Cercotrichas galactotes*), version 1.0. In Birds of
682 the World (J. del Hoyo, A. Elliott, J. Sargatal, D. A. Christie, and E. de Juana, Editors).
683 *Cornell Lab of Ornithology, Ithaca, NY, USA* (2020) doi:10.2173/bow.rutscr1.01.
684 53. Rashid, D. J. *et al.* From dinosaurs to birds: A tail of evolution. *Evodevo* **5**, 1–20 (2014).

685 54. Funston, G. F. *et al.* A new two-fingered dinosaur sheds light on the radiation of
686 Oviraptorosauria: Two-fingered oviraptorid. *R. Soc. Open Sci.* **7**, (2020).
687 55. Xu, X., Zheng, X. & You, H. Exceptional dinosaur fossils show ontogenetic development
688 of early feathers. *Nature* **464**, 1338–1341 (2010).
689 56. Wang, M., O'Connor, J. K., Xu, X. & Zhou, Z. A new Jurassic scansoriopterygid and the
690 loss of membranous wings in theropod dinosaurs. *Nature* **569**, 256–259 (2019).
691 57. Snively, E., Cotton, J. R., Ridgely, R. & Witmer, L. M. Multibody dynamics model of
692 head and neck function in *Allosaurus* (Dinosauria, Theropoda). *Palaeontol. Electron.* **16**,
693 (2013).
694 58. Hendrickx, C. *et al.* Morphology and distribution of scales, dermal ossifications, and other
695 non-feather integumentary structures in non-avialan theropod dinosaurs. *Biol. Rev.* (2022)
696 doi:10.1111/brv.12829.
697 59. Senter, P. & Robins, J. H. Resting orientations of dinosaur scapulae and forelimbs: A
698 numerical analysis, with implications for reconstructions and museum mounts. *PLoS One*
699 **10**, 1–21 (2015).
700 60. Vazquez, R. J. The automating skeletal and muscular mechanisms of the avian wing
701 (Aves). *Zoomorphology* **114**, 59–71 (1994).
702 61. Hutson, J. D. & Hutson, K. N. A test of the validity of range of motion studies of fossil
703 archosaur elbow mobility using repeated-measures analysis and the extant phylogenetic
704 bracket. *J. Exp. Biol.* **215**, 2030–2038 (2012).
705 62. Witmer, L. M. The extant phylogenetic bracket and the importance of reconstructing soft
706 tissues in fossils. in *Functional morphology in vertebrate paleontology* (ed. Thomason, J.
707 J.) 19–33 (Cambridge University Press, Cambridge, 1995).

63. Chimento, N. R. *et al.* Forelimb posture in Chilesaurus diegosuarezi (Dinosauria, Theropoda) and its behavioral and phylogenetic implications. *Ameghiniana* **54**, 567–575 (2017).
64. Novas, F. E. *et al.* An enigmatic plant-eating theropod from the Late Jurassic period of Chile. *Nature* **522**, 331–334 (2015).
65. Baron, M. G., Norman, D. B. & Barrett, P. M. A new hypothesis of dinosaur relationships and early dinosaur evolution. *Nature* **543**, 501–506 (2017).
66. Müller, R. T. & Dias-da-Silva, S. Taxon sample and character coding deeply impact unstable branches in phylogenetic trees of dinosaurs. *Hist. Biol.* **31**, 1089–1092 (2019).
67. Senter, P. Comparison of forelimb function between *Deinonychus* and *Bambiraptor* (Theropoda: Dromaeosauridae). *J. Vertebr. Paleontol.* **26**, 897–906 (2006).
68. Senter, P. & Robins, J. H. Range of motion in the forelimb of the theropod dinosaur Acrocanthosaurus atokensis, and implications for predatory behaviour. *J. Zool.* **266**, 307–318 (2005).
69. Senter, P. Forelimb function in Ornitholestes. *Palaeontology* **49**, 1029–1034 (2006).
70. White, M. A. *et al.* Forearm range of motion in *Australovenator wintonensis* (Theropoda, Megaraptoridae). *PLoS One* **10**, 1–20 (2015).
71. Sullivan, C., Hone, D. W. E., Xu, X. & Zhang, F. The asymmetry of the carpal joint and the evolution of wing folding in maniraptoran theropod dinosaurs. *Proc. R. Soc. B Biol. Sci.* **277**, 2027–2033 (2010).
72. Taewoo, K. *Orthoptera of Korea*. (Geobook, Seoul, Korea, 2013).
73. KIm, J. *The Odonata & Orthoptera, etc, of Korea*. (Kyohak, Seoul, Korea, 1998).
74. Lagos, P. A. A review of escape behaviour in orthopterans. *J. Zool.* **303**, 165–177 (2017).

75. Song, H. *et al.* 300 million years of diversification: Elucidating the patterns of orthopteran evolution based on comprehensive taxon and gene sampling. *Cladistics* **31**, 621–651 (2015).

76. O'Shea, M. & Williams, J. L. D. The anatomy and output connection of a locust visual interneurone; the lobular giant movement detector (LGMD) neurone. *J. Comp. Physiol.* **91**, 257–266 (1974).

77. Rind, F. C. & Simmons, P. J. Orthopteran DCMD neuron: A reevaluation of responses to moving objects. I. Selective responses to approaching objects. *J. Neurophysiol.* **68**, 1654–1666 (1992).

78. Burtt, E. H. *An analysis of physical, physiological, and optical aspects of avian coloration with emphasis on woodwarblers. Ornithological Monographs, No. 38.* (1986).

79. Savalli, U. M. *The evolution of bird coloration and plumage elaboration*. (In Current Ornithology, 1995).

80. Dimond, C. C., Cabin, R. J. & Brooks, J. S. Feathers, dinosaurs, and behavioral cues: Defining the visual display hypothesis for the adaptive function of feathers in non-avian theropods. *Bios* **82**, 58–63 (2011).

81. Cincotta, A. *et al.* Pterosaur melanosomes support signalling functions for early feathers. *Nature* **604**, (2022).

82. Jablonski, P. G. & Lee, S. Painted redstarts (*Myioborus Pictus*) attack larger prey when using flush-pursue strategy. *Open Ornithol. J.* **11**, 34–38 (2018).

83. R Core Team. A language and environment for statistical computing. R Foundation for Statistical Computing. (2021).

84. Dinno, A. Package 'dunn.test'. *CRAN Repository* 1–7 (2017).

85. Mangiafico, S. rcompanion: Functions to support extension education program evaluation. (2021).
86. Krapp, H. G. & Gabbiani, F. Spatial distribution of inputs and local receptive field properties of a wide-field, looming sensitive neuron. *J. Neurophysiol.* **93**, 2240–2253 (2005).
87. Shin, H. Escape Initiation Mechanism of Orthopteran Species as Anti-Predatory Adaptation. (Seoul National University, 2009).
88. Santer, R. D., Yamawaki, Y., Rind, F. C. & Simmons, P. J. Preparing for escape: An examination of the role of the DCMD neuron in locust escape jumps. *J. Comp. Physiol. A Neuroethol. Sensory, Neural, Behav. Physiol.* **194**, 69–77 (2008).
89. Judge, S. J. & Rind, F. C. The locust DCMD, a movement-detecting neurone tightly tuned to collision trajectories. *J. Exp. Biol.* **200**, 2209–2216 (1997).
90. Simmons, P. J., Rind, F. C. & Santer, R. D. Escapes with and without preparation: The neuroethology of visual startle in locusts. *J. Insect Physiol.* **56**, 876–883 (2010).
91. Fotowat, H., Harrison, R. R. & Gabbiani, F. Multiplexing of motor information in the discharge of a collision detecting neuron during escape behaviors. *Neuron* **69**, 147–158 (2011).
92. Gabbiani, F., Krapp, H. G. & Laurent, G. Computation of object approach by a wide-field, motion-sensitive neuron. *J. Neurosci.* **19**, 1122–1141 (1999).
93. Park, J., Lee, S. & Jablonski, P. G. Unpublished data.

Acknowledgements

We thank the Macaulay Library at the Cornell Lab of Ornithology for letting us use photos from their digital archives. We thank all the helpers, including: Jeongseop Lee, Hyein Jo, Seon-Yong

Lee, Yewon Yun, Hyo-hyun Kim, and Woojoo Kim. This work is part of the Doctoral Dissertation of Jinseok Park at the School of Biological Sciences, Seoul National University. This work was supported by Convergence grant 2019-2020 of Seoul National University, Korea; BK 21 grant to the School of Biological Sciences, Seoul National University, Korea; National Research Foundation of Korea funded by the Ministry of Education (no. 2022R1I1A2060919); DGIST R&D Program of the Ministry of Science and ICT (22-BRP-03), Korea.

Author contributions

S.L., P.G.J. established the hypothesis. H.M., Y.L., S.L., P.G.J. conceptualized this project and supervised the overall experiments. J.P., M.S., J.P., J.H., H.M., Y.L., S.L., P.G.J. contributed to the methodology. J.P. (Jinseok) and P.G.J. conducted field works with assistance from S.B. J.P. (Jinseok) conducted neurophysiological experiments, data curation and analysis, and visualization. H.M., Y.L., S.L., P.G.J. received grant funding. J.P., M.S., J.P. wrote the original draft. All authors commented on the draft.

Competing interests

Authors declare that they have no competing interests.

Data availability

All data are available in the supplementary tables.

Figure legends

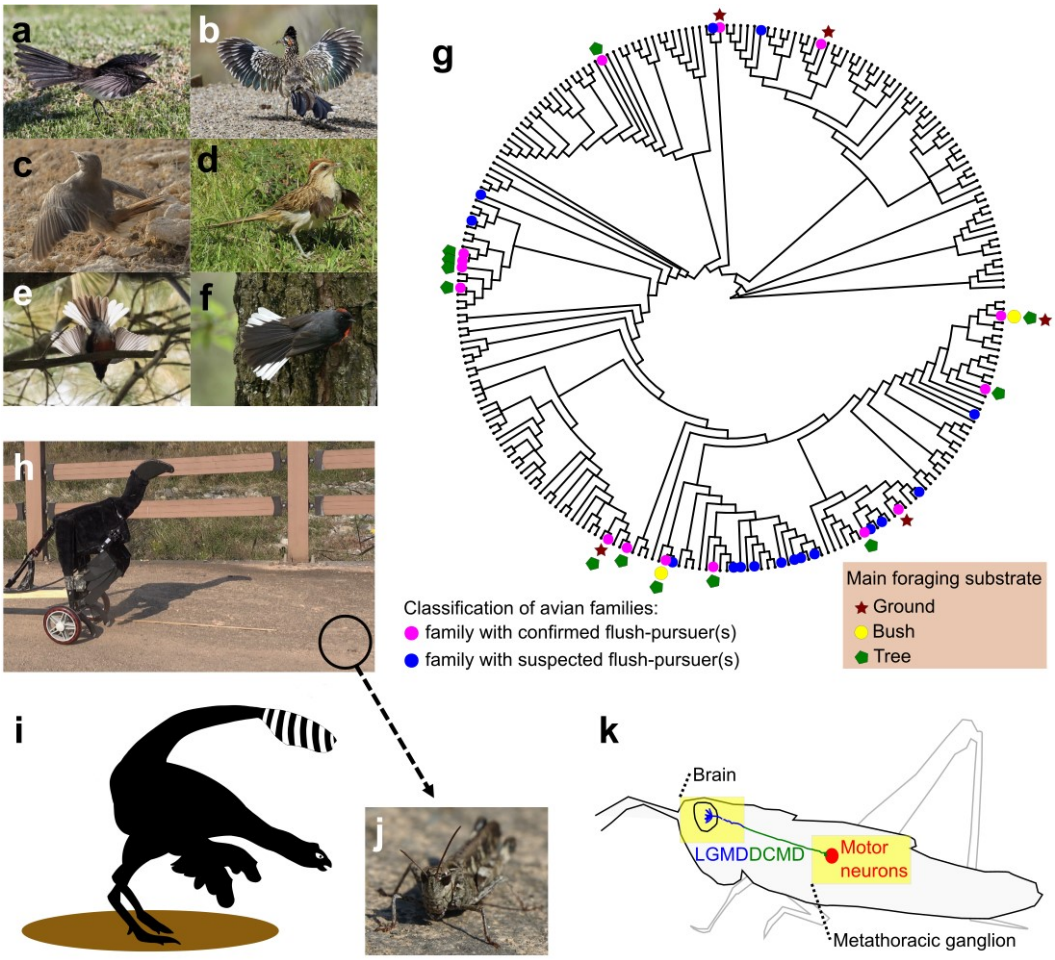

Fig. 1: Diversity of extant avian flush-pursuers, an example of their prey with simple neural escape pathways, and the Robopteryx imitating *Caudipteryx*.

a–**f**, Examples of flush-pursuers: *Rhipidura leucophrys*, *Geococcyx californianus*, *Cercotrichas galactotes*, *Tapera naevia*, *Myioborus pictus*, *Myioborus miniatus*, respectively [Macaulay Library: ML205494131, ML98307051, ML366333971, ML278048021, ML272399001, ML253368241 (more examples in Supplementary Note 1)]. **g**, Distribution of flush-pursuers among 248 avian families (see Extended Data Fig. 2 and Supplementary Note 1 for details). **h**, The Robopteryx in the natural habitat placed in front of the grasshopper. **i**, Artistic restoration of the hypothetical flushing by a feathered dinosaur. **j**, *Oedaleus infernalis* used in the experiments.

k, The looming-detecting neurons (LGMD/DCMD) involved in triggering the escapes in response to visual stimuli in orthopterans.

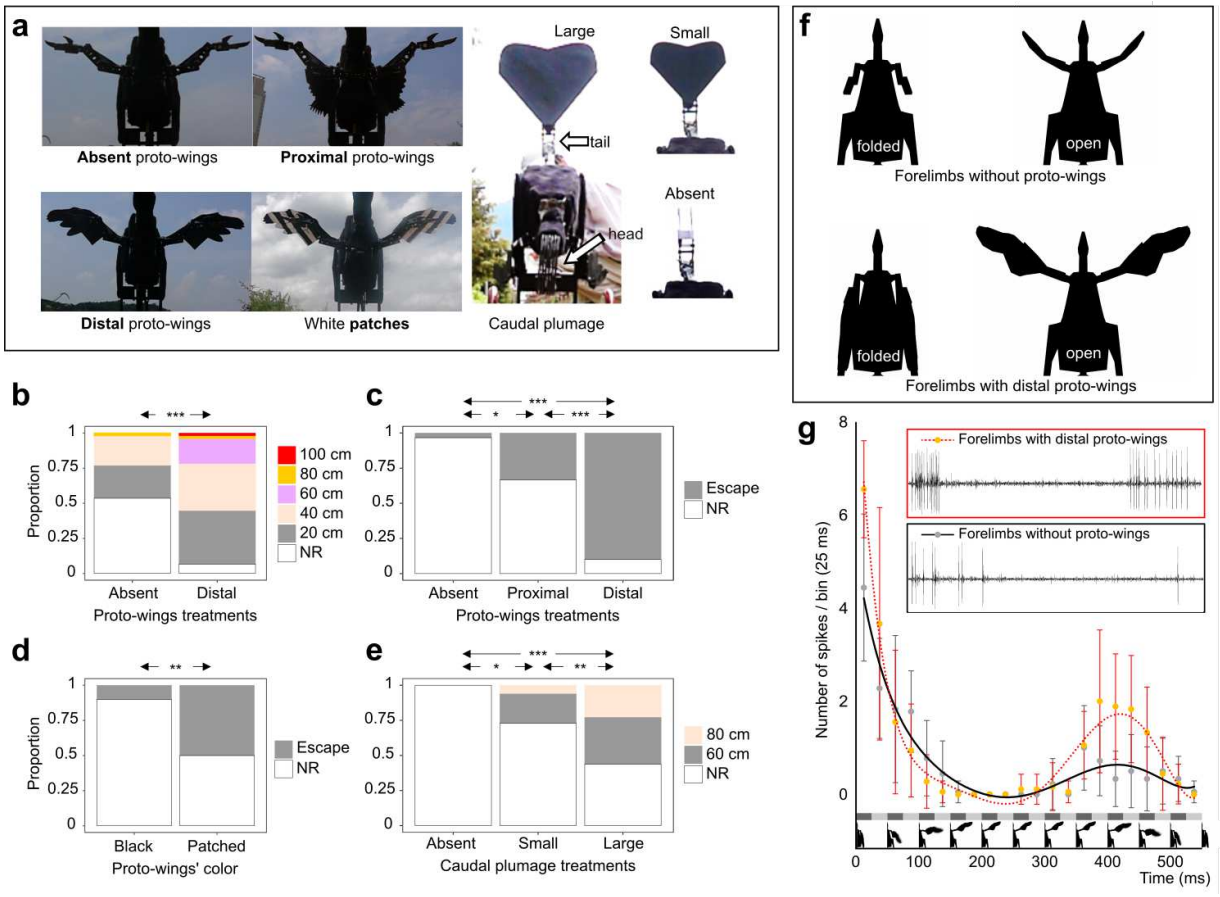

Fig. 2: Behavioral and neurophysiological experiments.

a, Experimental treatments in behavioral tests. **b**, The effect of the presence of the proto-wings on the escape frequency of grasshoppers at each of 5 distances: 100, 80, 60, 40, and 20 cm. **c**–**e**, The effect of the presence and location of proto-wings (**c**), their color (**d**), and the presence and size of caudal plumage (**e**) on the escape frequency of grasshoppers. NR means "no response." * indicates $P < 0.05$; ** indicates $P < 0.01$; *** indicates $P < 0.001$ (see Supplementary Tables 2–5 for details). **f**, Experimental treatments in neurophysiological experiments (the first frame and the most extended forelimbs of animation presented). **g**, The firing rate [nr of spikes/25 ms bin; average ± SD; n = 18 (6 recordings from each of 3 individuals)] of the grasshopper's escape pathway (LGMD/DCMD) in response to the animations without (solid black line) and with (dotted orange line) distal proto-wings (see Supplementary Tables 6 and 7). Bins are marked as

825 gray bars, and screenshots from the animation with proto-wings are shown at 50 ms intervals
826 along the horizontal axis. The insets represent two examples of the recorded responses (see
827 Extended Data Fig. 13 for details).
828

Extended Data

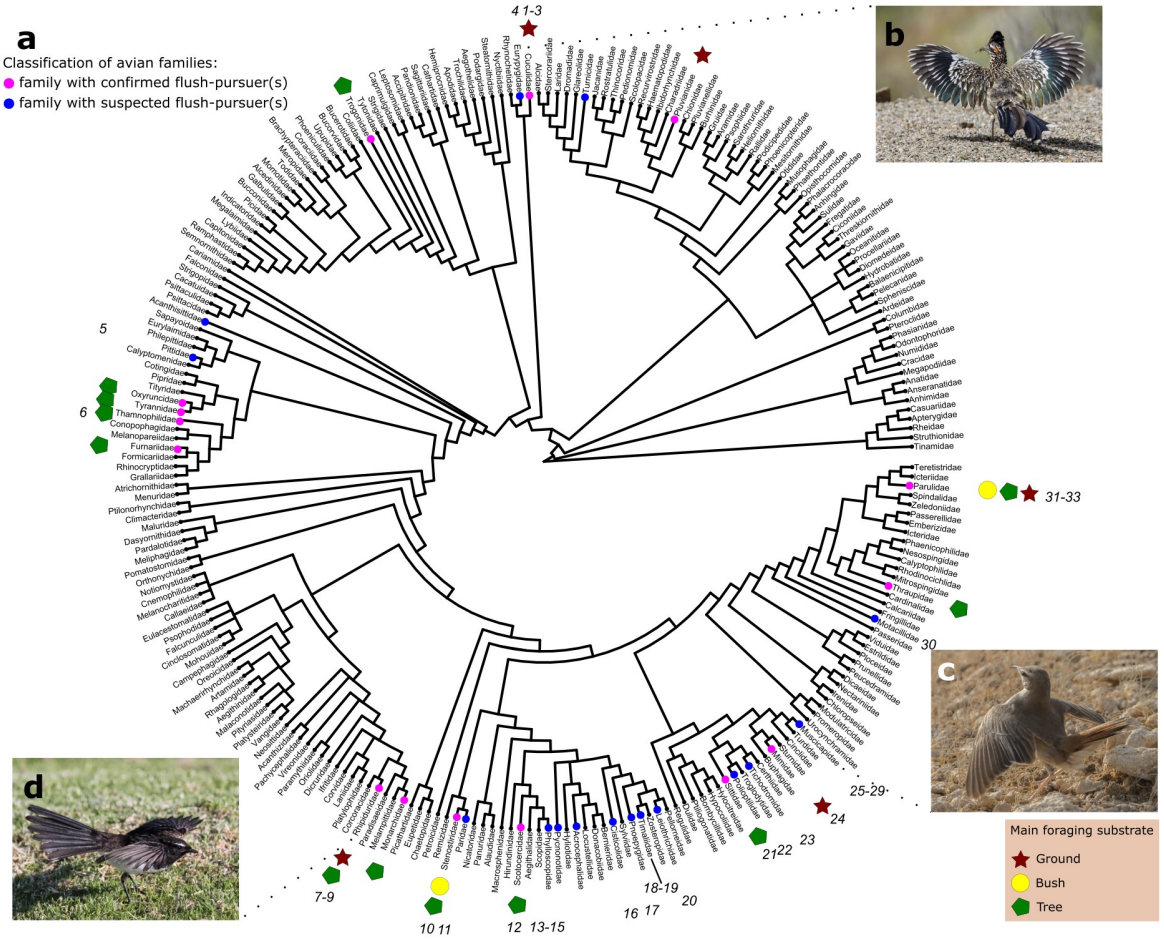

Extended Data Fig. 1: Phylogenetic distribution of extant avian flush-pursuers.

a, Phylogenetic distribution of extant flush-pursuers in 248 avian families[93]. Pink dots indicate families containing at least one species with evidence of using flush-pursue foraging and classified as "confirmed" flush pursuers (Supplementary Note 1). Blue dots indicate additional families containing at least one "suspected flush pursuer" (Supplementary Note 1) defined as an actively foraging species (i.e., not sit-and-wait predator) with evidence for the use of displays during foraging movements but with weaker evidence for direct links between the display and pursuing of the flushed prey (albeit video evidence suggesting the link may exist). Brown star,

yellow circle, and green pentagon denote the main foraging substrate of confirmed flush-pursuers within a family, and each means that the species mainly forage on the ground, in bushes, or trees, respectively. This consensus tree was built using a tree set obtained from BirdTree.org. **b**–**d**, Photos illustrating examples of displays of ground-foraging flush-pursuers: Greater Roadrunner (*Geococcyx californianus*), Rufous-tailed Scrub-Robin (*Cercotrichas galactotes*), Willie-wagtail (*Rhipidura leucophrys*) respectively from the following recordings in the Macaulay Library at the Cornell Lab of Ornithology: ML98307051, ML366333971, ML205494131. This figure concerns Fig. 1g. The numbers next to each family correspond to the numbers given to the links with flush-pursue foraging (in the internet movie archives such as Macaulay Library or YouTube) and listed in Supplementary Note 1. A comprehensive review of all avian species that include the flush-pursue foraging strategy among all the foraging strategies of a species will be the subject of a separate review paper[93].

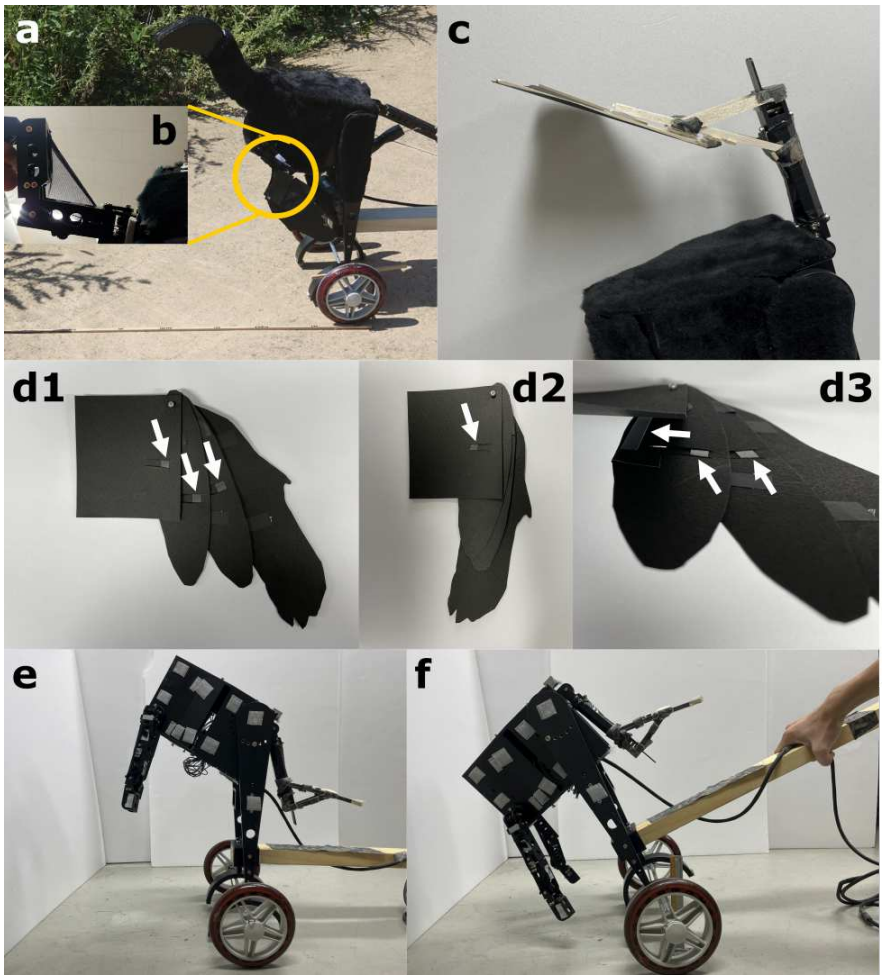

Extended Data Fig. 2: Details on the *Caudipteryx* robot (Robopteryx).

a, For behavioral experiments, the main body and legs of the robot were covered with black felt. The head was built from black-colored polystyrene. **b**, A surface made of dark stockings was used to imitate propatagium. **c**, An additional structure was attached to the robot's tail to imitate a bending tail. **d1**–**d3**, Paper distal proto-wing used in experiments 1 to 3. White arrows indicate plastic pieces attached onto pieces of proto-wing to control the minimum (**d2**) and maximum (**d1**) range of movement of each piece of proto-wing. **e**, The main body of the robot was tilted 37° upward for experiments concerning the proto-wings (Experiments 1 to 3) to imitate a flush pursuer position similar to the observed ground-foraging flush-pursuers (e.g., *Geococcyx californianus*; link 1 in Supplementary Note 1) **f**, The main body of the robot was tilted 40°

862 downward for an experiment concerning caudal plumage (experiment 4) to imitate a situation in
863 which the upward movements of the tail may potentially affect on the grasshopper; otherwise,
864 that tail is behind the body and not visible to the grasshopper. This posture is also observed
865 among foraging birds, especially if they already focus on a specific ground area in front of them.

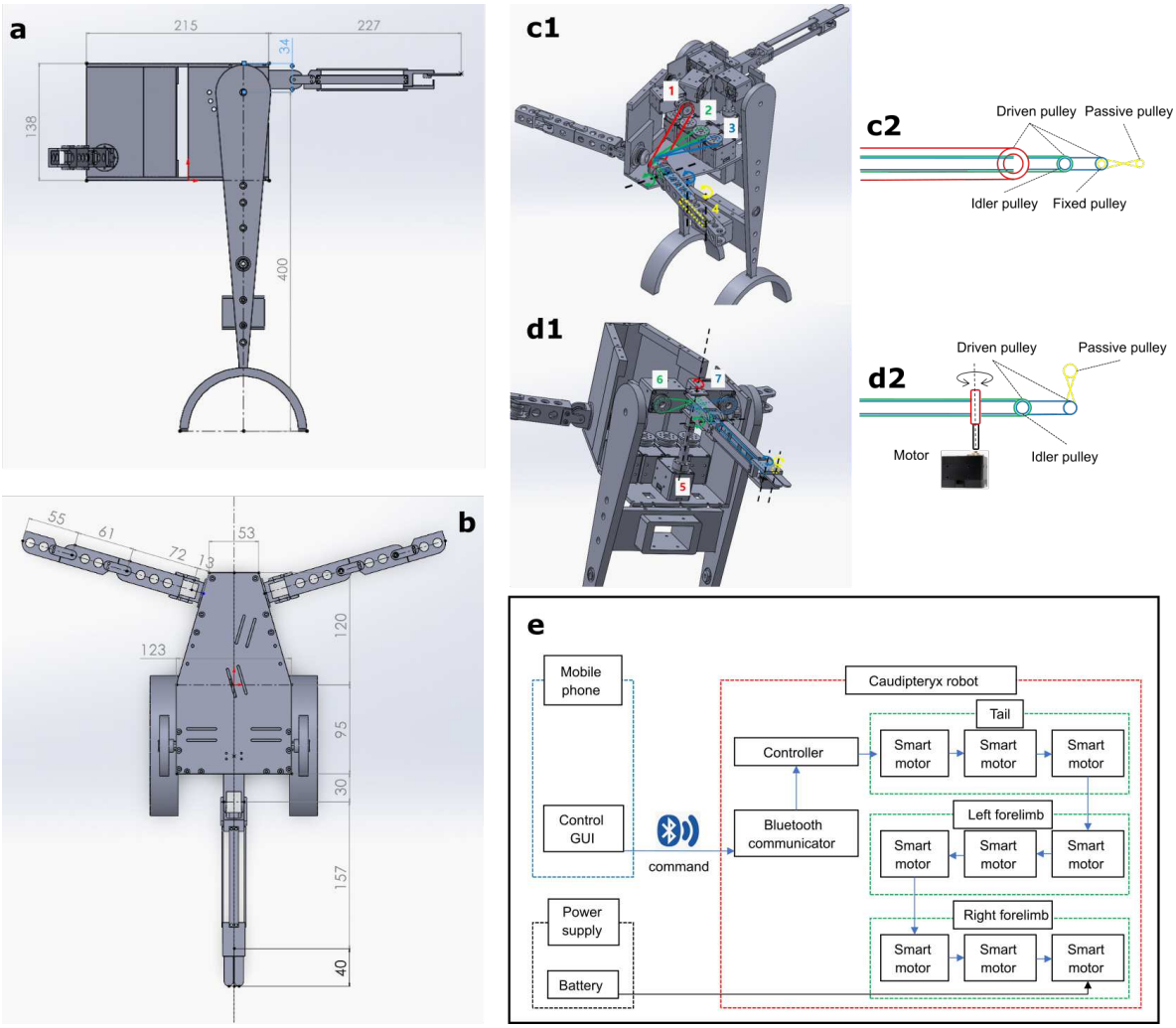

866

867 **Extended Data Fig. 3: Hardware and control system of the *Caudipteryx* robot (Robopteryx).**

868 **a**, Side view of CAD model used to build the Robopteryx. **b**, Top view of CAD model used to

869 build the Robopteryx. The unit of length shown is mm. **c1** and **c2**, For the forelimb motion, two

870 fishing lines and a belt are used as tendons in controlling motion for the pitch (green), yaw (blue),

871 and roll (red) rotation. The fishing line (blue) connected with motor no.3 also implements

872 rotating at the elbow joint. An additional fishing line (yellow) is used in rotating the wrist joint

873 passively. **d1** and **d2**, For the tail motion, a motor (no.6) with a fishing line (green) is used to

874 control the pitch motion. We implement the yaw rotation (motor no.5) and spread the tip of the

875 tail (blue) in the robot. **e**, The schematic diagram of the robot control system. The controller

876 receives operation commands created from a mobile phone through the Bluetooth communicator.
877 The controller is connected to a series of smart motors. An external battery is used to supply the
878 power.

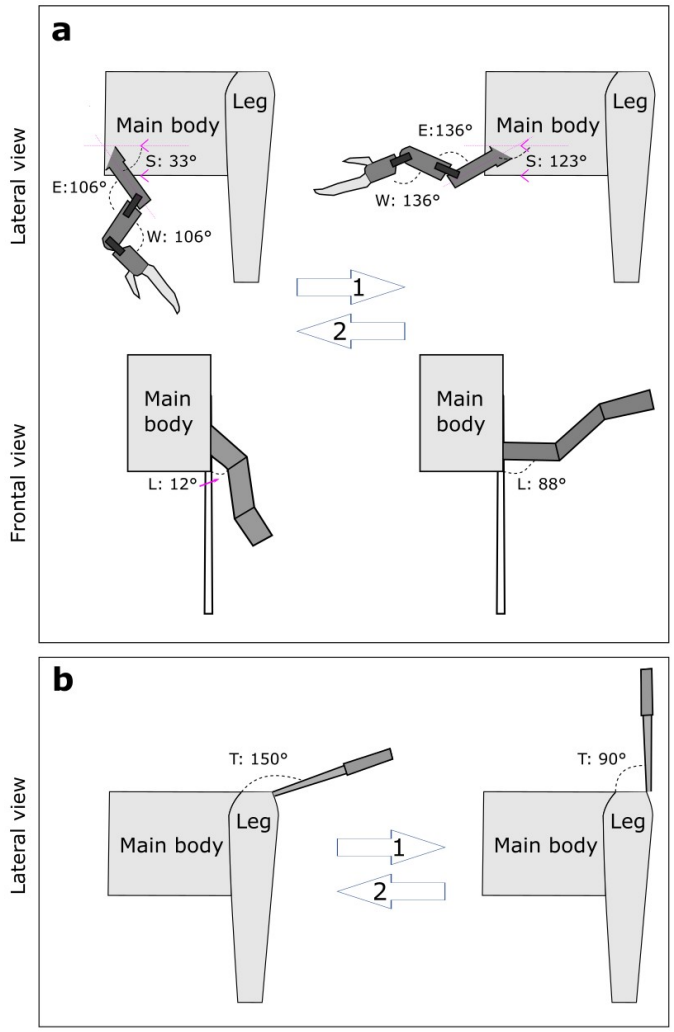

879

880 **Extended Data Fig. 4: Motion ranges of the Robopteryx's flushing movements chosen for**

881 **the experiments performed in this study.**

882 **a**, The proto-wings' flushing movements start from the resting posture (33° in S, 106° in E, 106°

883 in W, 12° in L) to the estimated maximum values of each angle (arrow 1; 123° in S, 136° in E,

884 136° in W, 88° in L) and then revert to the resting posture (arrow 2). **b**, For the tail's flushing

885 movement, the robot lifts its tail (arrow 1; angle T changes from 150° to 90°) and lowers it

886 (arrow 2; angle T changes from 90° to 150°). For tail experiments, the main body is tilted to

887 imitate an animal lowering its head to search for prey on the ground and displaying with its tail

888 when the prey may actually detect the upward-lifting movements of the tail.

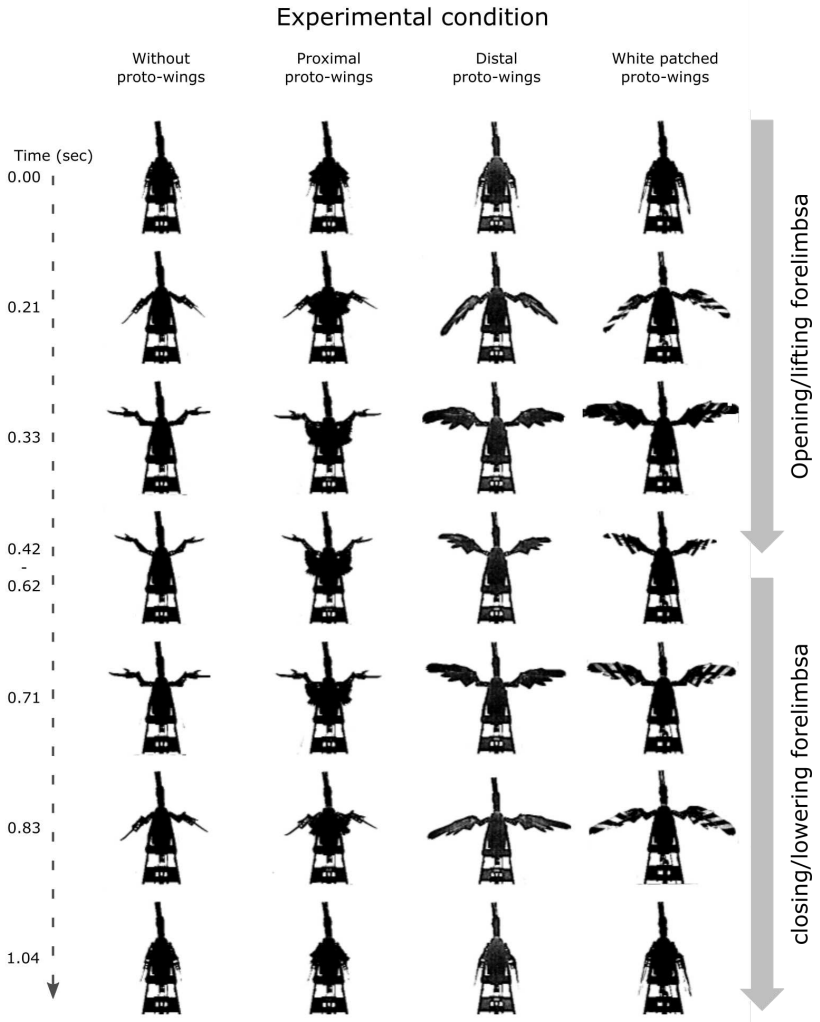

889

890 **Extended Data Fig. 5: The Robopteryx's forelimb movements viewed from the point of**

891 **view of the grasshopper.**

892 Each of the four columns (from left to right) represents a series of frames showing the robot

893 displays in the four experimental treatments (proto-wings absent, proximal proto-wings present,

894 distal proto-wings present, and white patches present on distal proto-wings) filmed from the

895 grasshopper point of view on the ground level 40 cm away from the robot (from the mid-point

896 between the robot's leg). The bottom panels show the resting posture at the end of the movement.

897 The vertical broken arrow on the left represents the time in seconds.

898

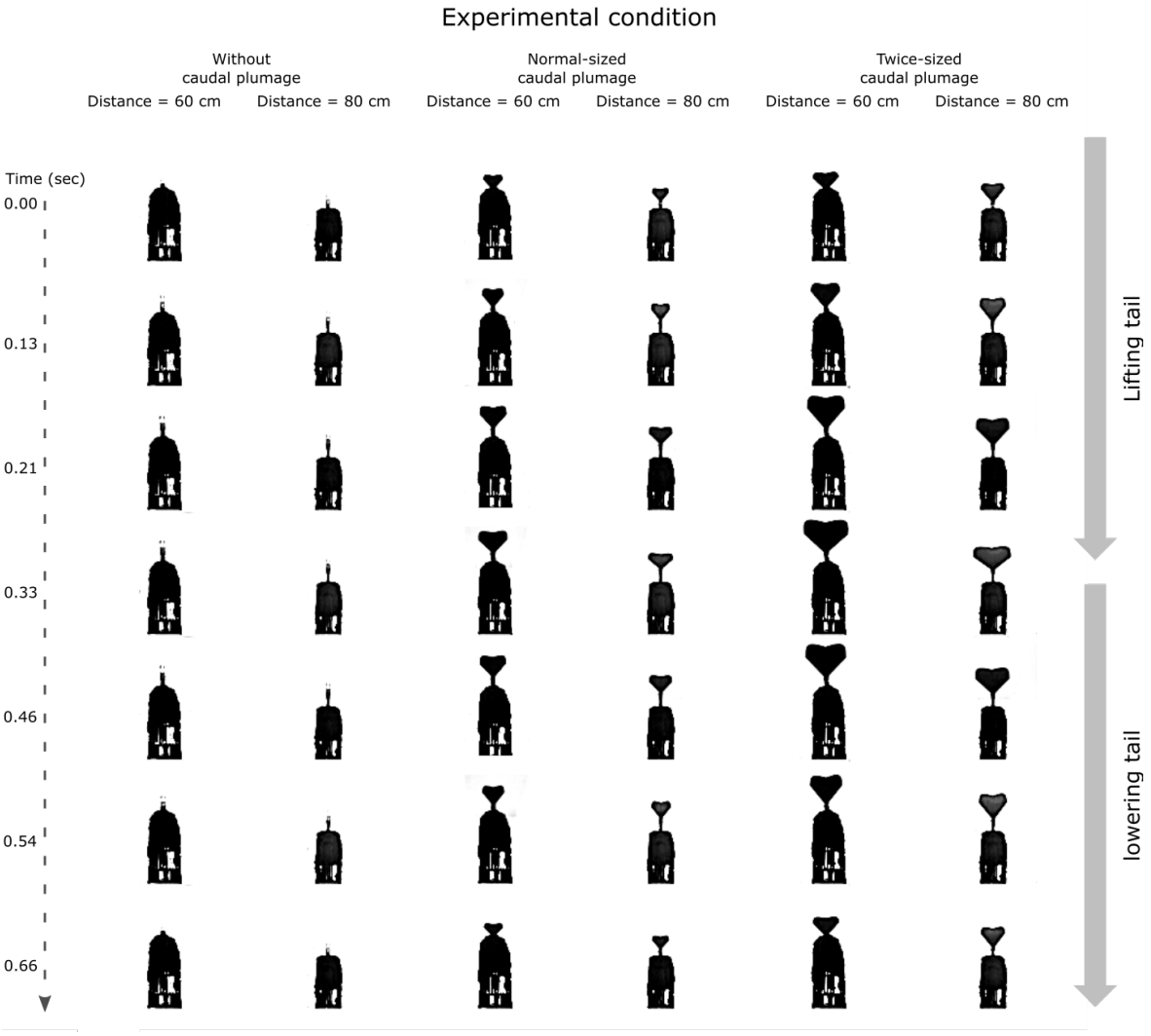

Extended Data Fig. 6: The Robopteryx's tail movements viewed from the point of view of the grasshopper.

Each of the three pairs of columns (from left to right) represents a series of frames showing the robot displays in the three experimental treatments (caudal plumage absent, normal-sized caudal plumage present, and the large-sized caudal plumage present) filmed from the grasshopper points of view on the ground level at 60 and 80 cm away from the and the robot (from the mid-point between the robot's leg). The bottom panels show the resting posture at the end of the movement. The vertical broken arrow on the left represents the time in seconds.

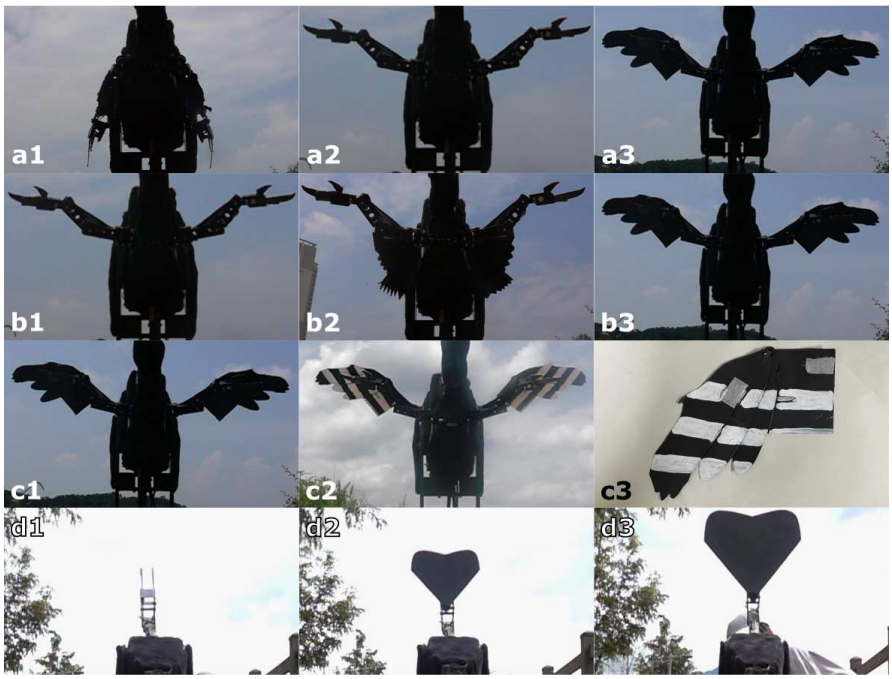

Extended Data Fig. 7: Experimental designs of the behavioral experiments.

a1–**a3**, Experimental treatments in Experiment 1: (**a1**) motor sound without forelimbs' movement; (**a2**) proto-wings absent; (**a3**) distal proto-wings present as in the fossil records of *Caudipteryx*. **b1–b3**, Experimental treatments in Experiment 2: (**b1**) proto-wings absent; (**b2**) proximal proto-wings present; (**b3**) distal proto-wings present. **c1** and **c2**, Experimental treatments in Experiment 3: (**c1**) plain black proto-wings; (**c1**) white-patched proto-wings. (**c3**) Close-up view of the hypothetical proto-wing with white patches used in Experiment 3. **d1–d3**, Experimental treatments in Experiment 4: (**d1**) caudal plumage absent; (**d2**) caudal plumage present; (**d3**) large caudal plumage present.

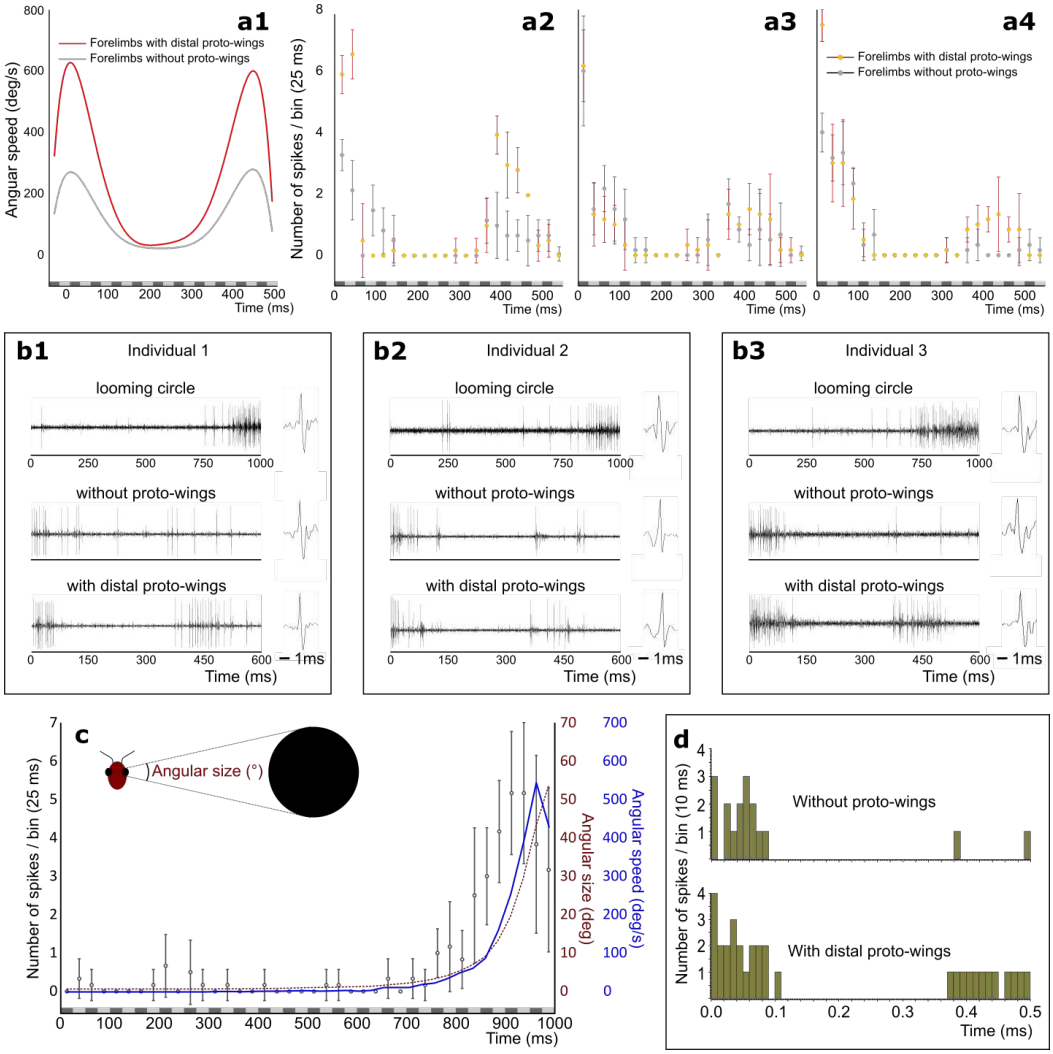

Extended Data Fig. 8: Results of neurophysiological experiments.

a1, Angular speed calculated from the forelimb tips' movements in the *Caudipteryx* animations (Supplementary Videos 6 and 7). **a2–a4**, The firing rate (nr of spikes/25 ms bin; average ± SD) of the looming-sensitive escape pathway from each of three individuals in response to the animations of forelimbs display without (gray bar; n = 6) and with (red bar; n = 6) distal proto-wings. All records from three individuals are used in Fig. 1g. Bins are marked as gray bars along the horizontal axis. **b1–b3**, Examples of recordings from the grasshopper' LGMD/DCMD looming-detective pathway from each of three individuals in response to animations: a looming circle; forelimb movement without proto-wings; forelimb movement with proto-wings. A spike

930 next to a recording is an example from that recording. Spike shapes slightly differed between
931 individual grasshoppers (especially in terms of the amplitude of the lower and upper part of the
932 spike), but the spike shapes were similar between the looming circle and the animations of flush
933 displays within the same individual grasshopper. A comprehensive study of the
934 neurophysiological responses to a full variety of hypothetical displays by flush-pursuing
935 dinosaurs will be a subject of a separate paper. The spike data is shown in Supplementary Tables
936 6 and 7. **c**, The firing rate in response to a looming circle. The firing rate (nr of spikes/25 ms bin;
937 average ± SD) of the grasshopper looming-sensitive escape pathway in response to a looming
938 circle animation [n = 6 (2 recordings from each of three individuals)]. The approaching speed
939 was 6 m/s. The right-side Y-axis shows the stimulus angular size (deg; dotted burgundy line) and
940 speed (deg/s; solid blue line) of the looming circle. Bins are marked as gray bars along the
941 horizontal axis. The spike data is shown in Supplementary Table 9. **d**, Examples of the firing rate
942 of the escape pathway analyzed with the bin size of 10 ms to show that even with a short bin size,
943 the peak value of spiking frequency occurs right at the outset of the flush display animation. The
944 remaining analyses were conducted using a bin size of 25 ms to decrease random variation
945 among bins.
946

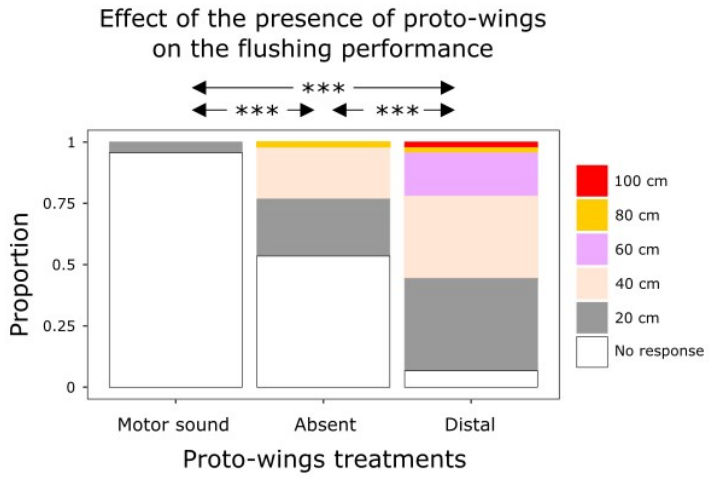

Extended Data Fig. 9: Confirmation that the robot's sound does not affect grasshopper escapes.

The effect of the motor sound created during the robot's movement and the effect of the presence of the proto-wings on the forelimbs on the flushing performance in Experiment 1. Y axis shows the proportion of grasshoppers that escaped at each distance: 100, 80, 60, 40, and 20 cm during a procedure involving repeated displays by the robot at 20cm distance intervals starting at 100 cm and ending at the distance at which the grasshopper jumped or at 20cm, and classifying the outcome as "NR" (no response) if the grasshopper did not escape even at the 20cm. This figure concerns Fig. 2b. *** indicates $P < 0.001$ according to the Dunn's test with Bonferroni correction ["*dunn.test*" function in dunn.test package in R[84]]. The data are shown in Supplementary Table 2.

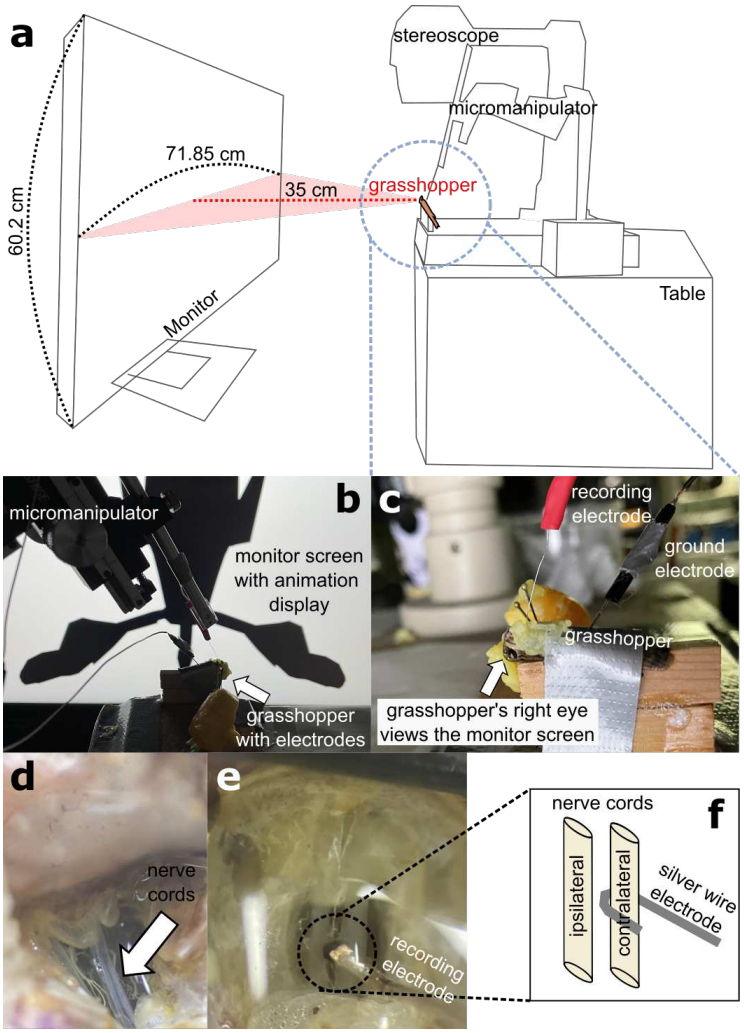

Extended Data Fig. 10: Experimental set-up for neurophysiological experiments.

a, Schematic view of the experimental set-up for neurophysiological experiments. A grasshopper and equipment are placed on a table. The distance between the monitor and the grasshopper's right eye is set to 35 cm. **b**, *Caudipteryx* animation is displayed on the monitor. **c**, The silver wire hook-electrode (red – recording electrode) wrapped around the contralateral ventral nerve cord, and a pin (black – ground electrode) in the grasshopper's abdomen connected to the ground. **d**, An arrow indicates the ventral nerve cords of the grasshopper. **e** and **f**, A dotted circle indicates the point of the ventral nerve cord where the electrode is hooked to the contralateral nerve cord.

Supplementary Files

This is a list of supplementary files associated with this preprint. Click to download.

- SupplementaryVideoLegends.docx
- Video5.mp4
- Video7.mp4
- Video4.mp4
- SupplementaryInformation.pdf
- Video1.mp4
- Video6.mp4
- Video2.mp4
- Video3.mp4